Schweizerische Eidgenossenschaft
Confédération suisse
Confederazione Svizzera
Confederaziun svizra

Federal Department of the Environment, Transport, Energy and Communications DETEC

Swiss Federal Office of Energy SFOE
Dam Safety section

A PROPOSAL FOR HORIZONTAL AND VERTICAL ELASTIC DESIGN SPECTRA

Input for the new Swiss code for dams

Technical Report

SED/BFE/R/01/30072015

Poggi Valerio, Donat Fäh

Swiss Seismological Service
ETH Zurich

Thursday 30th July, 2015

This feasibility study has been commissioned by the Swiss Federal Office of Energy (*Bundesamt für Energie*, BFE) in the frame of the "Erdbebengefährdung für die Revision der Richtlinie zur Stauanlagensicherheit".

The documents and relative material has to be cited as following:

Poggi Valerio and Donat Fäh (2015), *A proposal for horizontal and vertical elastic design spectra. Input for the new Swiss code for dams.* Swiss Seismological Service, ETH Zurich. Technical report SED/BFE/R/01/06072015.

Contents

Chapter 1

Introduction

1.1 Motivation

In the framework of the definition of the new building code for dams, the Swiss Federal Office for Energy (BFE, Bundesamt für Energie) requested the Swiss Seismological Service (SED) to perform a study on the effect of site response variability on elastic design spectra for different soil conditions and seismic hazard scenarios. The final goal of this study is the definition of a set of site-dependent design spectra for the horizontal and vertical components, whose design shape (scaled to PGA) is to be compared with the present normative.

To accomplish the task, a set of Fourier amplification functions are initially converted to response spectral amplification functions using a combination of spectral modeling techniques and random vibration theory. The analysis is performed for different SIA soil classes (A to E) and for a set of magnitude-distance combinations, representative of the Swiss hazard deaggregation scenario at the Sion site and for return periods of 500, 1000, 5000 and 10000 years. In a second step, the response spectral amplification functions for each soil class and scenario are combined with the corresponding uniform hazard spectra (on rock) in order to obtain site-dependent hazard curves. Finally, new design spectral shapes are calibrated for the different SIA classes, accounting for scenario variability including some level of conservatism.

To account for epistemic uncertainty, different strategies for the calculation of the response spectral amplification functions are considered, including site-specific ground motion models (from measured and stochastically generated velocity profiles) and direct (empirical) observations. The process follows a rather complex logic tree approach, which is summarized in figure 1.1; details of the whole process are given in the next chapters. Note that, at the time of this report, the 2015 Swiss Hazard Model is still undergoing a review process and the information presented herein are subject to changes.

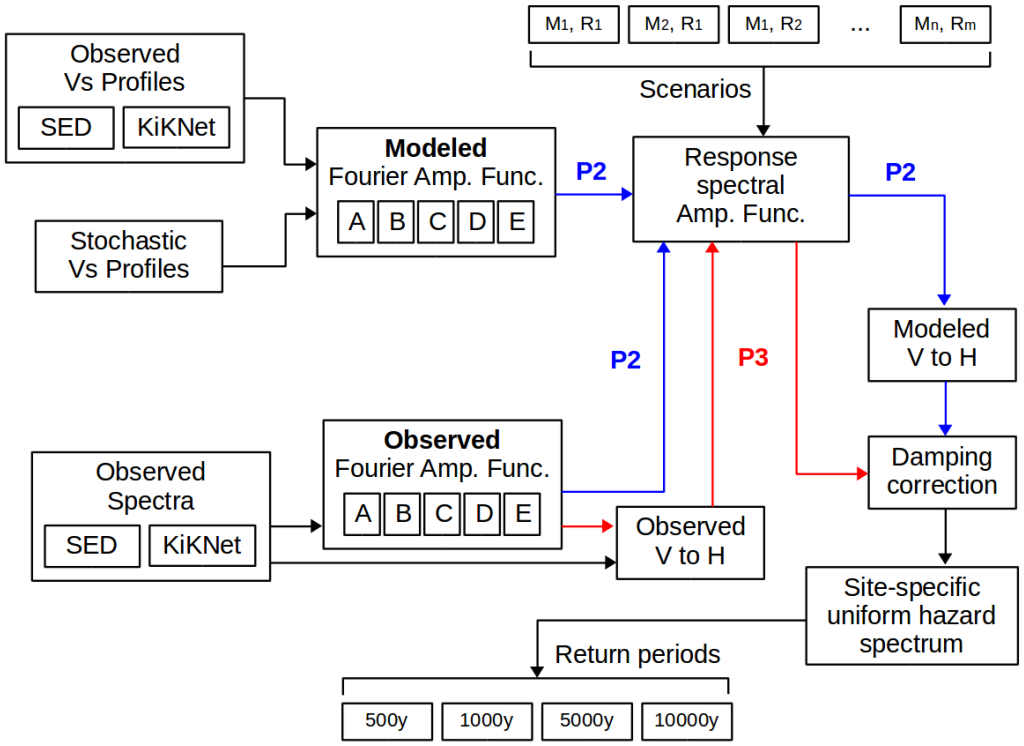

Figure 1.1: Schematic representation of the processing tree to compute site dependent uniform hazard spectra using different strategies.

1.2 Note on presentation of results

For the sake of conciseness, not all the results for each combination of method, class and scenario are represented in the manuscript. A selection of best representative examples is given instead, to allow the reader understanding the basics of the procedure. Nonetheless, all data and related pictures for all the steps of this study are made available as an electronic attachment to this document.

In the manuscript we often alternate frequency and period representation of spectral quantity. This is done in order to facilitate the separation of information. For example, amplification functions (either Fourier and response spectral) are better presented in frequency domain to highlight features which are relevant in site response analysis. Conversely, hazard and design spectra are generally presented in period, for compatibility with the standard engineering representation.

Chapter 2

S-wave Velocity Profiles

2.1 SIA 261 classification

To account for the variability of ground motion amplification on different soil conditions, the classification scheme from SIA 261 normative (revision 2014) has been used to group sites of expected similar seismic response. The SIA 261 normative prescribe six separated soil classes (A to F) of progressively decreasing stiffness. However, special class F could not be exploited within this study, due to lack of calibration data, and is therefore neglected from further analysis.

The SAI 261 classification scheme is based on direct geological/geotechnical description of the surface geology and on the use of indirect geotechnical and geophyscial proxies. The most relevant proxies for our purposes is the travel-time average S-wave velocity over the first $30m$ (Vs_{30}), which is considered in literature a parameter highly correlated with site amplification. In this study, we use the Vs_{30} at each analyzed site to discriminate between classes A to D (see Table 2.1 for class specific velocity bounds). Class E required a more elaborated analysis of the velocity profiles, accounting for the presence of large velocity gradients at shallow depths (5 to 20m).

	A	*B*	*C*	*D*	*E*
Vs30 Min.	800	500	300	100	100
Vs30 Max.	2500	800	500	300	500

Table 2.1: Vs30 upper and lower bounds (units in m/s) for the definition of SIA 261 classes used in this study.

A)

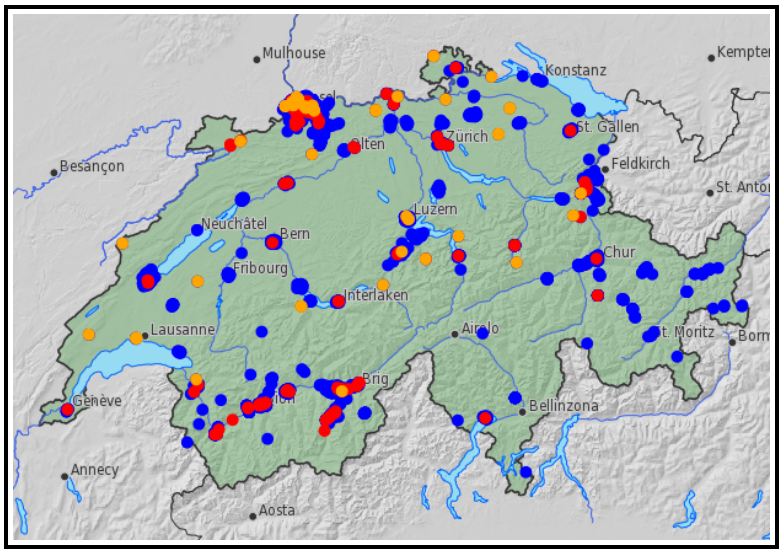

B)

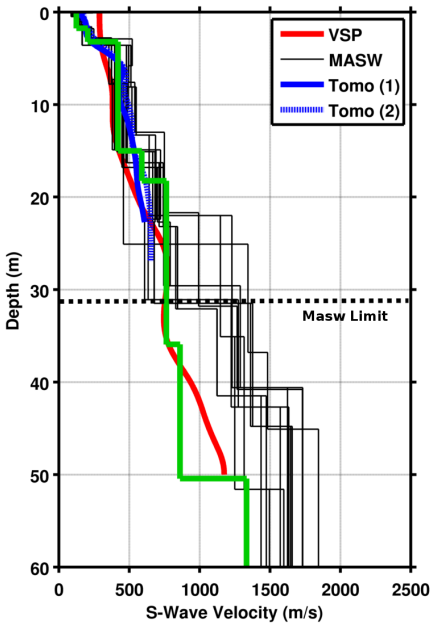

Figure 2.1: A) Location of sites of the SED site characterization database. In blue the sites with H/V spectral ratio only; in red the sites with array measurement of ambient vibration (and H/V spectral ratios); in orange the sites investigated with active seismic techniques (MASW). B) Example of characterized S-wave velocity profiles for the SED station STIEG (active and passive analysis).

2.2 The S-wave velocity profile collection

For the calculation of amplification function from modeling we primarily target the velocity profiles available from the SED site characterization database. However, the number of measured velocity profiles available from the SED database is not sufficient to fully represent the variability of site conditions in all SIA classes. In particular, class E is poorly represented, mostly due to the present criteria of site selection for the Swiss network (see figure 2.3 at the end of this chapter). Moreover several profiles for class A are affected by a considerable uncertainty, due to the difficulties in performing measurement on rock conditions (particularly when using ambient vibration analysis).

To overcome such lack of information, additional datasets have been included in the analysis: the Japanese KiKNet network and a synthetic dataset of stochastically generated velocity profiles. In the following the main characteristics of the three collections are presented.

2.2.1 Swiss site-characterization database

The SED site characterization database consists of a collection of 181 sites (figure 2.1A) investigated using both ambient vibration methods (127) and active seismic techniques (54) or both. Part of these sites are at the location or close to a seismic station of one of the Swiss networks (SSMNet and SDSNet). Presently 67 stations have also velocity profiles at the site of the installation. Additional 70 stations are planned and will be characterized in the frame of the SSMNet renewal project *Phase II* (2013-2019).

Those velocity profiles from surface wave analysis of ambient vibrations are the most reliable and can reach considerable depths (commonly $> 100m$). However, S-wave profiles investigated with active seismic techniques (MASW) are in few cases less reliable, due to the difficult measuring conditions (hard rock sites), and the low penetration depth of the method ($< 30 - 35m$, e.g. figure 2.1B), which make necessary some extrapolation to large depth (Poggi et al., 2013a).

2.2.2 Japanese KiKNet strong motion database

The Japanese KiK-net strong-motion network (Aoi et al., 2004) includes a collection of velocity profiles (P and S) from 689 sites of the network. These profiles

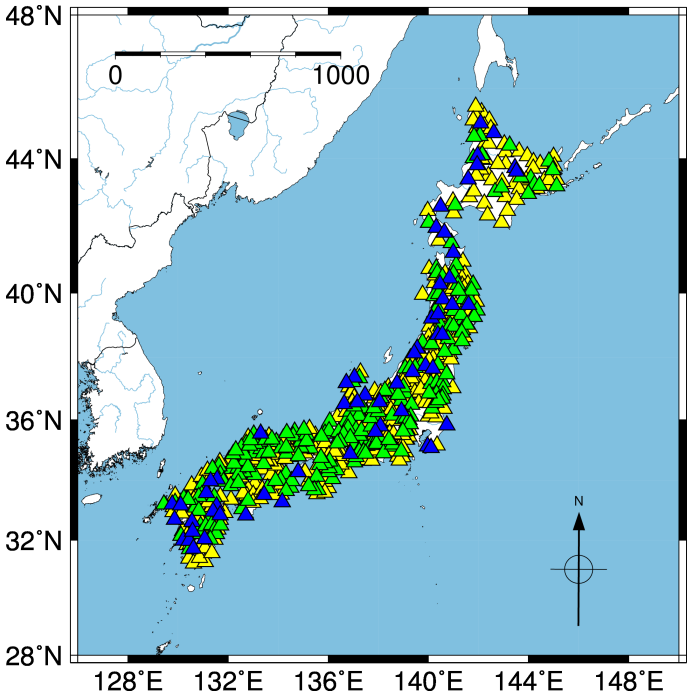

Figure 2.2: Distribution of stations of the KiK-Net Japanese strong motion network with available S-wave velocity profile. Blue and green triangles are respectively the selected rock and soft sediment sites; in yellow those sites rejected from interpretation.

were provided by the Japanese National Research Institute for Earth Science and Disaster Prevention (NIED) and were obtained from downhole logging in boreholes set up for the installation of buried sensors. The KiK-net velocity profiles are quite simple, often represented with very few (average) layers. This is generally not a problem when high frequency ground motion is analyzed, but amplification models at high frequencies can suffer from this oversimplification. This issue will be better developed later in this study. Note also that the KiK-Net network includes only a small number of very soft soil conditions due to the site selection criteria.

From the whole dataset with 689 sites, a subset of 220 soft sediment sites and 69 rock sites was extracted and analyzed in this study. The sites were selected based on the comparison of empirical amplification functions and H/V spectral ratios with modeled amplification functions from the 1D velocity profiles. For more details about the selection refer to (Poggi et al., 2012a) and (Poggi et al., 2013b).

2.2.3 A synthetic dataset based on Vs30 distribution

To investigate the variability of the site response a set of stochastically generated velocity profiles was produced. The randomization process is based on Vs_{30}. For each class, 100 random realization of Vs_{30} are first generated within the bounds prescribed by the SIA 261 normative (see Tab. 2.1). Subsequently, synthetic profiles are constructed for a given Vs_{30} using a stochastic approach. This is advantageous since many profiles with similar (or same) Vs_{30} can be produced, but with generally different velocity distribution over depth, and therefore different site response.

The procedure to generate synthetic profile for a specific Vs_{30} value is described as follow. Given a prescribed number of layers (here ten), an initial random distribution of velocities and layer thickness is generated (the starting model), according to the conditional constraints of velocity increasing with depth and with parameters ranging within a-priory prescribed bounds (dependent on the site class). A bedrock interface is also modeled for those sites with $Vs < 800m/s$ by including a variable velocity contrast (of max. $1500m/s$) at random depth location. For class E however such interface is forced to range between $5m$ and $20m$ only and with a velocity of the bedrock not lower than 800 m/s. The generated profile is eventually adjusted using a linearized optimization algorithm to exactly match the prescribed input Vs_{30} value.

Profiles obtained in such a way are realistic (figure 2.5), being gradient like (due to conditional constraints) but including as well significant velocity jumps, as for the effect of sediment-bedrock (or sediment-sediment) interfaces. The distribution of randomly generated Vs_{30} values for each SIA class can be seen in figure 2.8.

	A	*B*	*C*	*D*	*E*
Swiss DB	31	58	53	33	6
KiKNet	61	182	212	97	55
Syn. DB	100	100	100	100	100

Table 2.2: Number of sites with velocity profiles in each SIA class for the different databases used in this study.

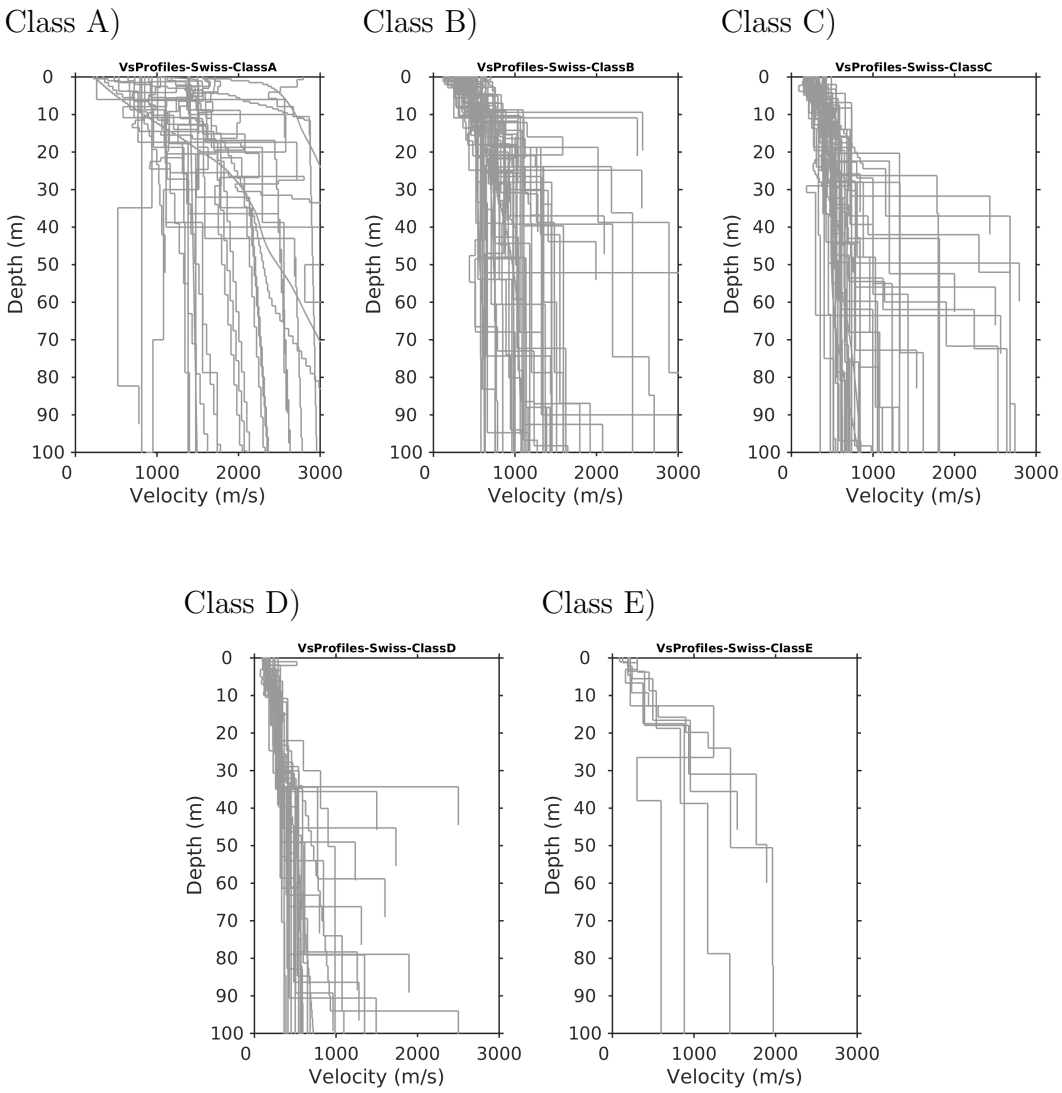

Figure 2.3: Comparison of the S-wave velocity profiles from the SED site-characterization database grouped in different SIA soil classes.

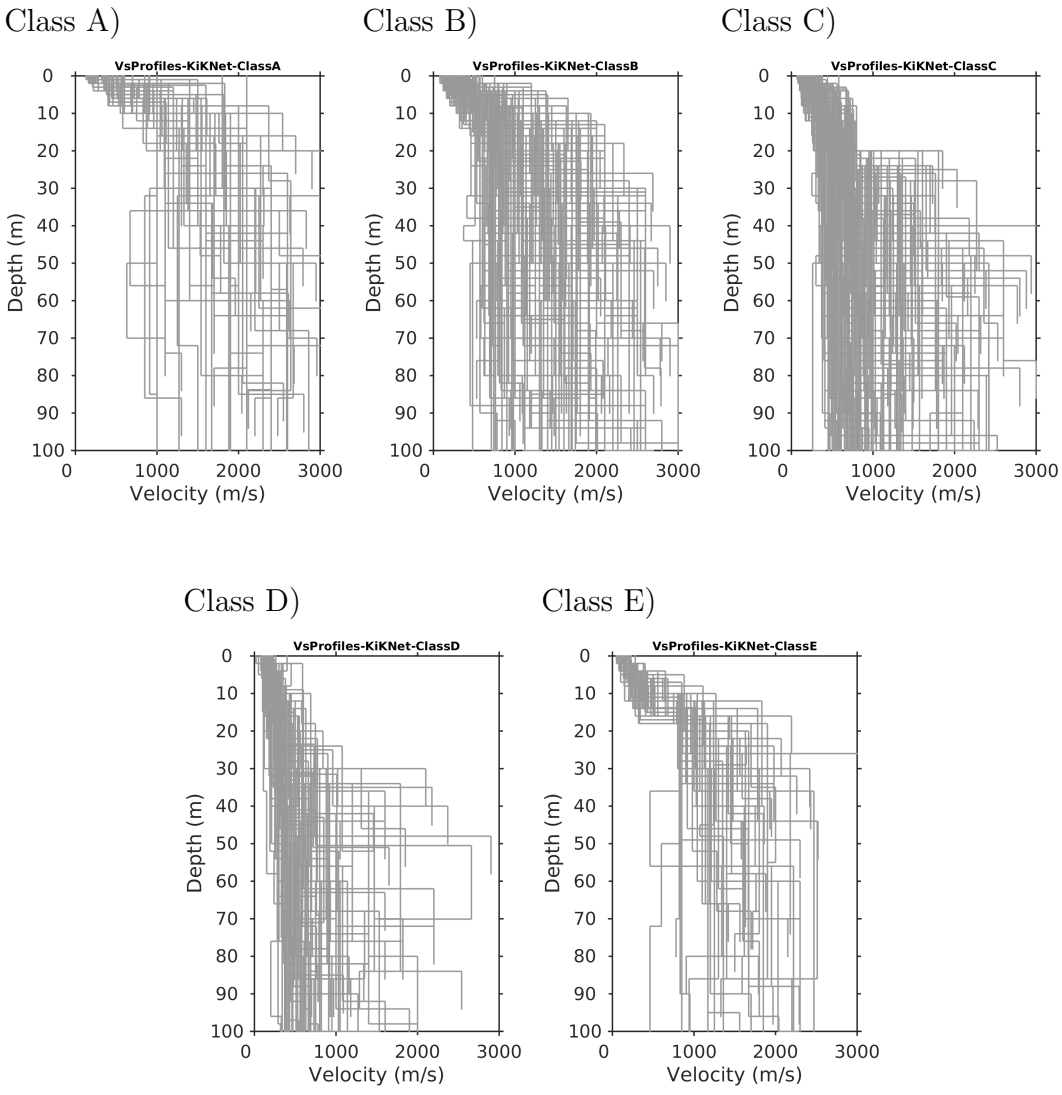

Figure 2.4: Comparison of the S-wave velocity profiles from the Japanese KiK-Net strong motion database grouped in different SIA soil classes.

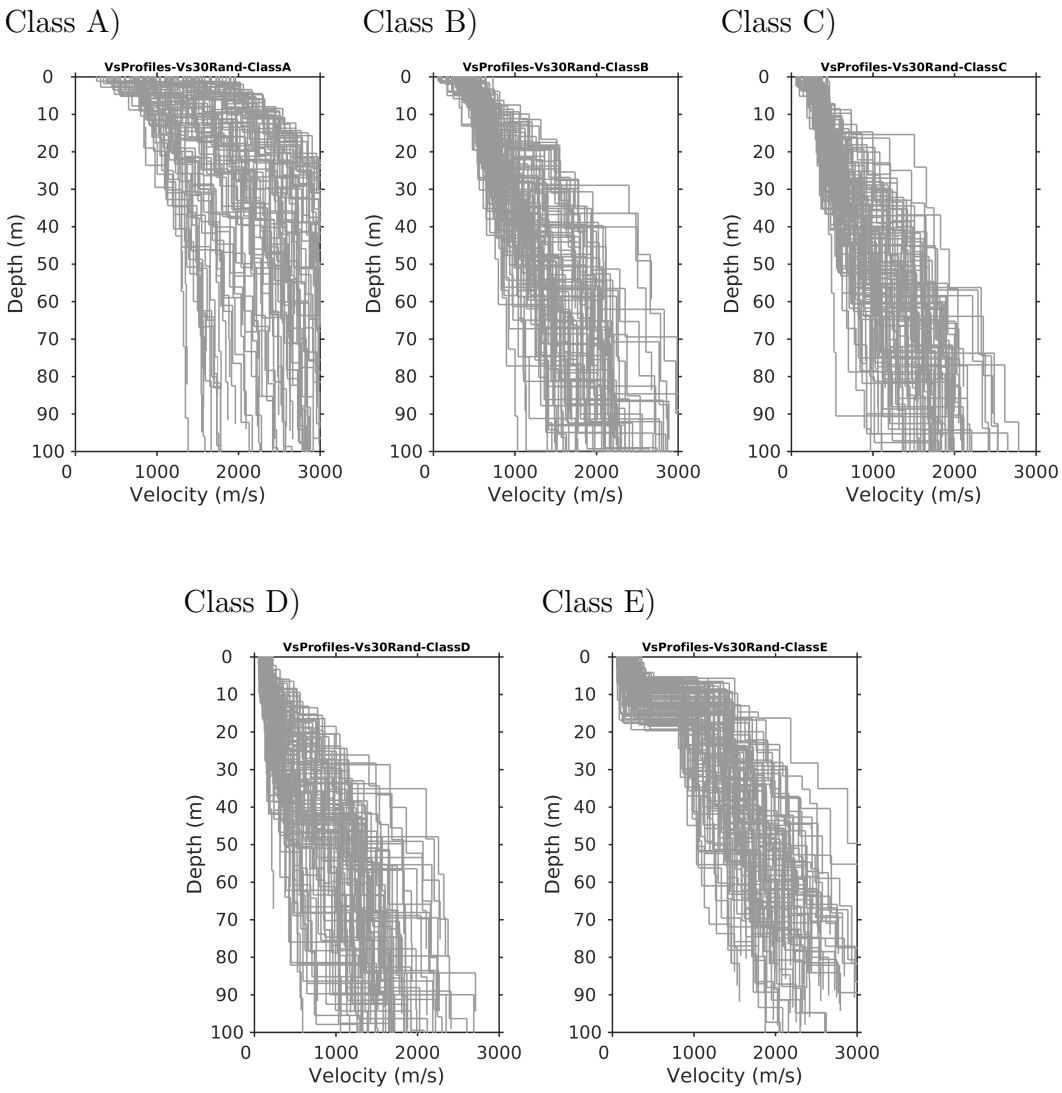

Figure 2.5: Comparison of stochastically generated S-wave velocity profiles grouped in different SIA soil classes.

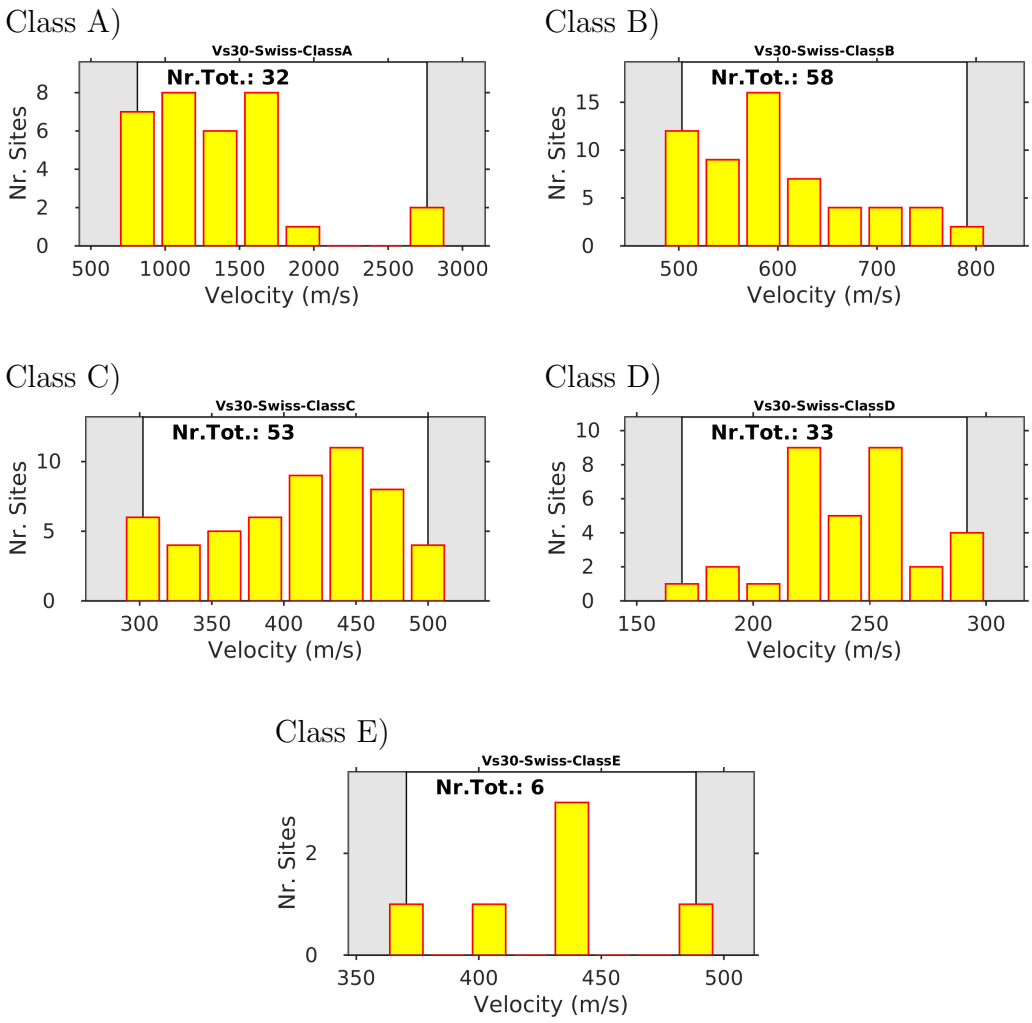

Figure 2.6: Distribution of Vs_{30} values for the stations of the SED database for the different SIA soil classes. Vs_{30} bounds are as for Tab. 2.1

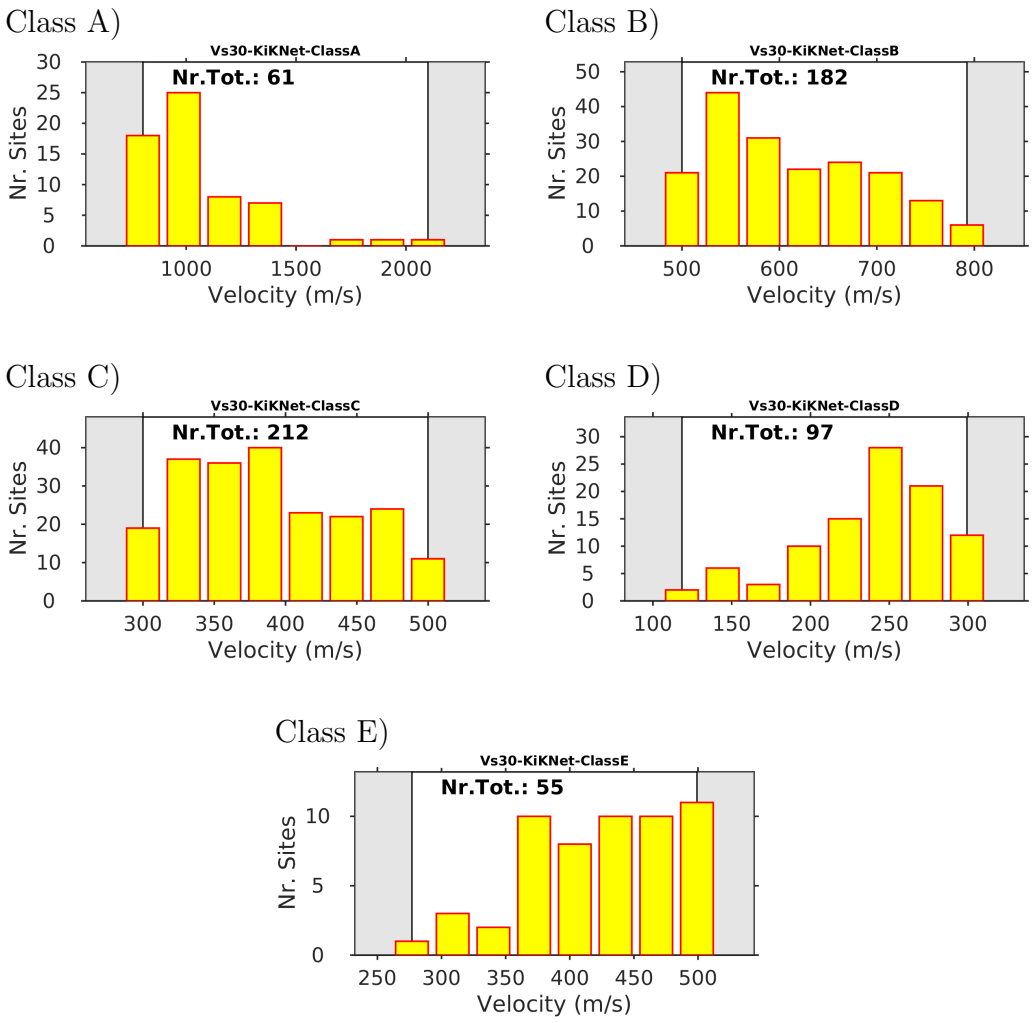

Figure 2.7: Distribution of Vs_{30} values for the stations of the japanese KiK-Net database for the different SIA soil classes. Vs_{30} bounds are as for Tab. 2.1

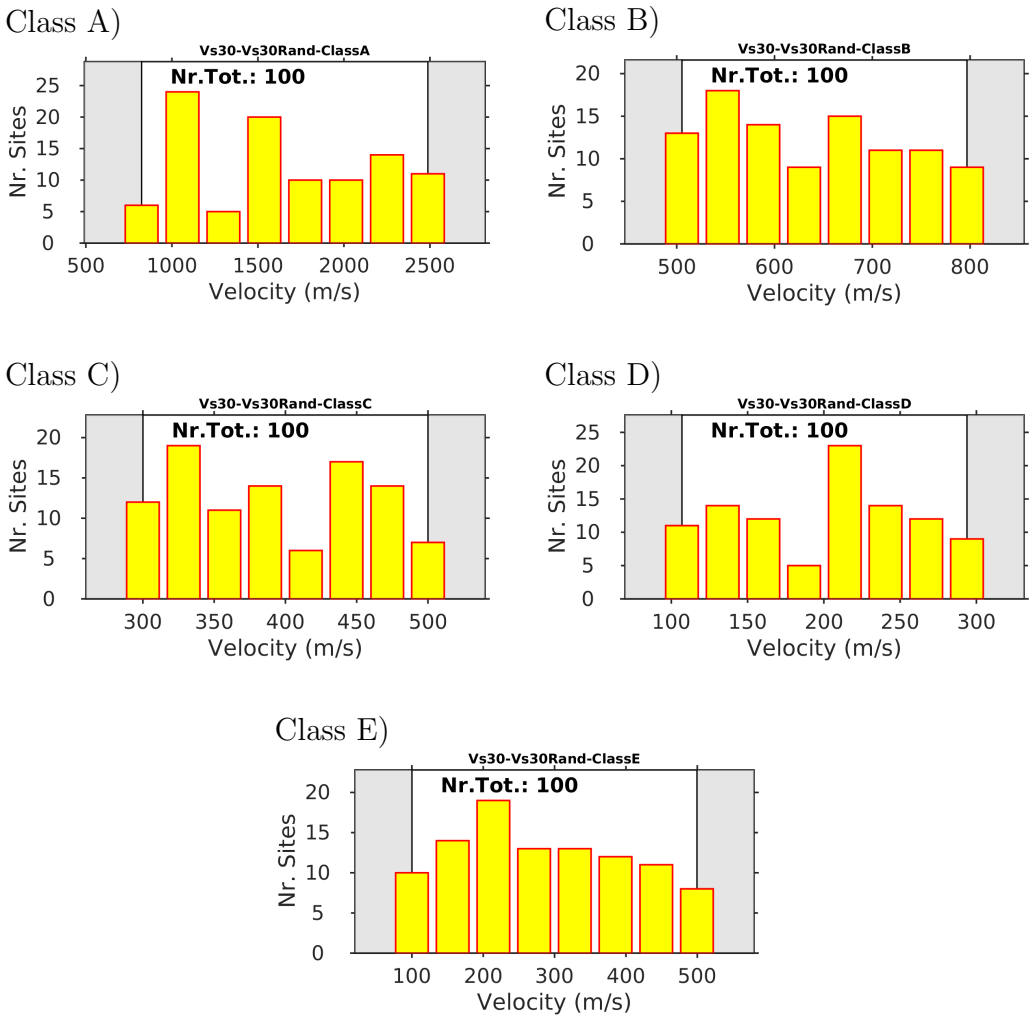

Figure 2.8: Distribution of randomly generated Vs_{30} values of the stochastic database for the different SIA soil classes. Vs_{30} bounds are as for Tab. 2.1

Chapter 3

Fourier Amplification Functions

3.1 Empirical amplification functions

For each real-time station of the Swiss networks (SSMNet, SDSNet) an empirical estimate of the local amplification (both elastic and anelastic) and its related uncertainty are available. Empirical site amplification functions are obtained at each site from a procedure of spectral modeling and inversion of a large number of small-magnitude events. This procedure is a by-product in the development of stochastic ground-motion prediction equation for Switzerland (Edwards et al., 2011; Edwards and Fäh, 2013a).

The method consists in the definition of a reference spectrum modeled using the event-specific inverted source characteristics and regional ground-motion attenuation models for each station. The general form of source and path effects can be described through a regional ground motion prediction equation (GMPE) providing the spectral shape on a reference velocity structure as a function of a number of parameters (corner frequency or stress drop, seismic moment and distance, regional Q-model and geometrical spreading model, reference near site attenuation term, etc.).

A generalized inversion scheme is needed to derive the different model parameters simultaneously over a large number of stations of the network and a large number of events. The advantage is that for a specific event, the source characteristics are common over the different stations, while for a specific station, site amplification can be considered constant between events of similar characteristic. Such redundancy reduces the non-uniqueness of the inverse problem, giving the possibility to better constrain the model parameters and minimizing the trade-off with the estimation of the local site-amplification factors, which are then obtained as the residual between observed and modeled spectral shapes.

3.2 The QWL amplification model

The SED has proposed several studies about the implementation of local amplification predictors based on the comparison between observed empirical amplifications and site-specific proxies. In this study we refer to the method proposed by Poggi et al. (2011) and Poggi et al. (2012b), which is based on the calculation of two quarter-wavelength (QWL) parameters: the average velocity (Vs^{Qwl}) and the impedance contrast (IC^{Qwl}).

The quarter-wavelength average velocity was initially proposed by Joyner et al. (1981), and subsequently optimized by Boore (2003), and consists in travel-time average of the elastic parameter down to a depth corresponding to 1/4 of the wavelength of interest. Such estimate is therefore frequency dependent and is suited to be related to the specific site amplification in the different frequency bands.

However, using the quarter-wavelength average velocity alone is not sufficient to characterize the variability of the ground-motion at soft sediment sites. Spectral amplification induced by resonance is related to the contrast of the seismic impedance at depth. For this reason, we introduced the concept of quarter-wavelength seismic impedance contrast (Poggi et al., 2012a). Such parameter gives the possibility of directly relating the largest seismic velocity contrasts of a velocity profile with resonance amplification.

The correlation to seismic site response has then been exploited by comparing empirical (anelastic) amplification functions from spectral modeling and quarter-wavelength parameters for a set of selected sites of the Japanese KiK-Net strong motion network. From the analysis we derived a simple functional form (equation 3.1) to predict frequency-dependent amplification factors in the range 0.5-20Hz at any site with a one-dimensional velocity profile of sufficient depth.

$$A(f) = exp(a(f)log(Vs^{Qwl}(f)) + b(f)log(IC^{Qwl}(f)) + c(f)). \tag{3.1}$$

The values of the frequency dependent coefficients a, b and c of equation 3.1 are presented in table 3.1. Using this approach we have modeled anelastic Fourier amplification functions for all the sites of the Swiss and Japanese databases with available velocity profile (e.g. figure 3.1) and for all the synthetic S-wave velocity profiles from stochastic simulation.

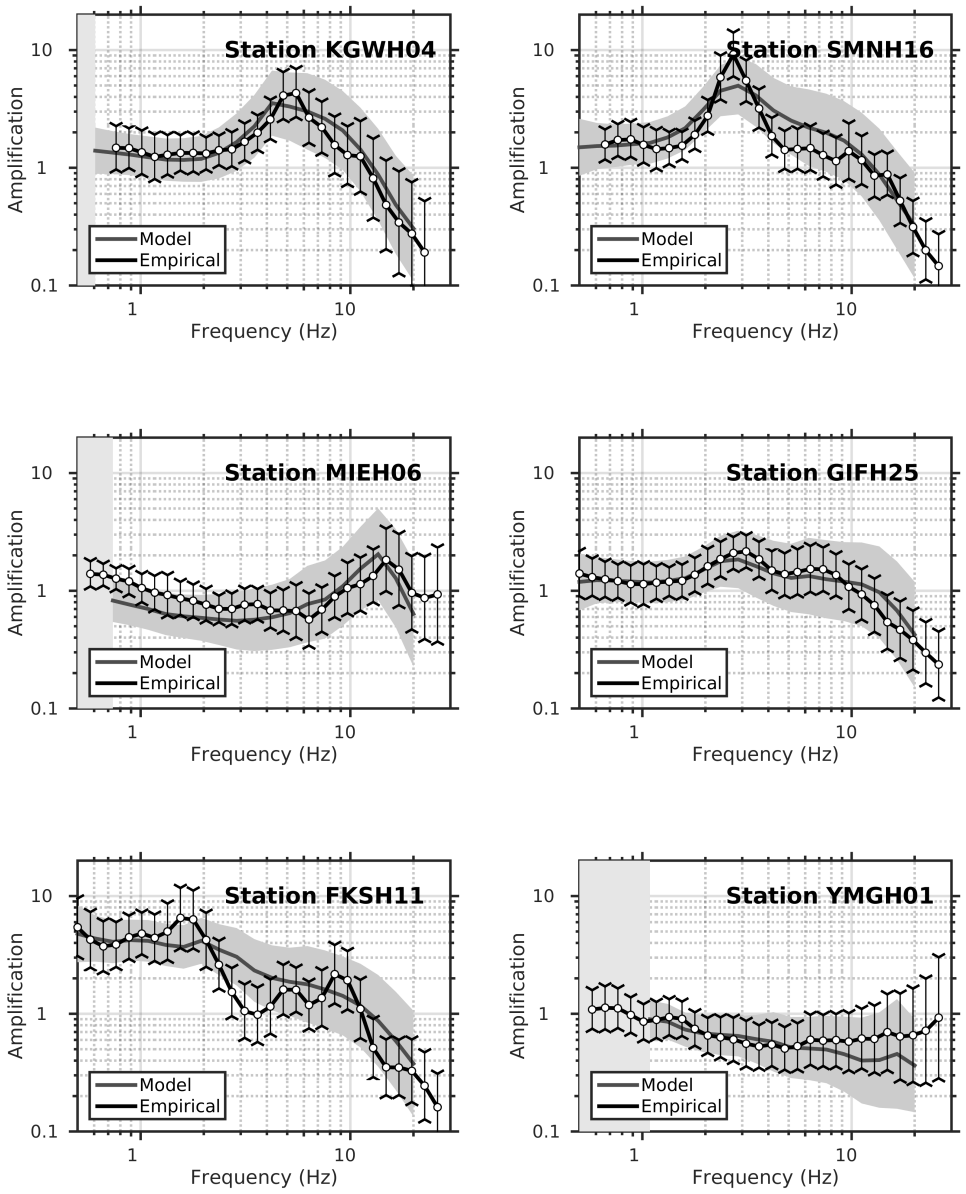

Figure 3.1: Comparison between amplification functions from spectral inversion (empirical) and modeling using the quarter-wavelength parameters (model) at different sites of the Japanese KiK-Net network.

$Freq.(Hz)$	a	b	c	$Std.Dev.$
0.5000	-1.22343021	-0.09253728	9.33123794	1.74583268
0.6071	-1.11197660	-0.23564151	8.51657322	1.57108930
0.7372	-1.06373934	-0.21171599	8.08744397	1.52088470
0.8952	-1.10196139	-0.23563287	8.28666344	1.49371848
1.0870	-1.09345790	-0.25167924	8.12311413	1.50346784
1.3200	-1.03314722	-0.08190246	7.51212602	1.51062331
1.6028	-0.99945603	-0.11252443	7.18289346	1.53062641
1.9463	-0.93887908	-0.07426708	6.64489353	1.56715689
2.3633	-0.82918214	0.14424344	5.67542095	1.64688093
2.8697	-0.78990921	0.22503225	5.26358993	1.75377631
3.4847	-0.75058333	0.25561919	4.88743599	1.84644394
4.2313	-0.72504056	0.27363343	4.61506951	1.89035900
5.1380	-0.68004352	0.28229386	4.27374641	1.94908695
6.2390	-0.59734476	0.29105031	3.75415800	2.11275645
7.5759	-0.58572901	0.38997457	3.54586918	2.14787210
9.1993	-0.48971738	0.46415892	2.85661243	2.16327385
11.1705	-0.24196712	0.46821897	1.31263144	2.26742291
13.5641	0.04217755	0.56457828	-0.53854378	2.45169460
16.4707	0.26928134	0.48532613	-2.10539861	2.61387313
20.0000	0.31820171	0.36880777	-2.75905104	2.80810875

Table 3.1: Coefficients used in equation 3.1 for the calculation of amplification factors from quarter-wavelength parameters.

3.3 The SH-wave transfer function

In case of the horizontally layered velocity structures, resonance patterns are predictable using simplified approaches. In particular, the SH-wave transfer function ($SHtf$) is calculated as a spectral ratio between modeled ground motion at the surface with respect to the bedrock at depth considering vertical incident plane wave (however, any arbitrary angle of incidence is possible as well). Absolute value of the SH-transfer function is the amplification function of the site assuming local reference. To make the estimation comparable between different locations, the local transfer function has then to be adjusted to a regional rock reference profile (Edwards and Fäh, 2013a).

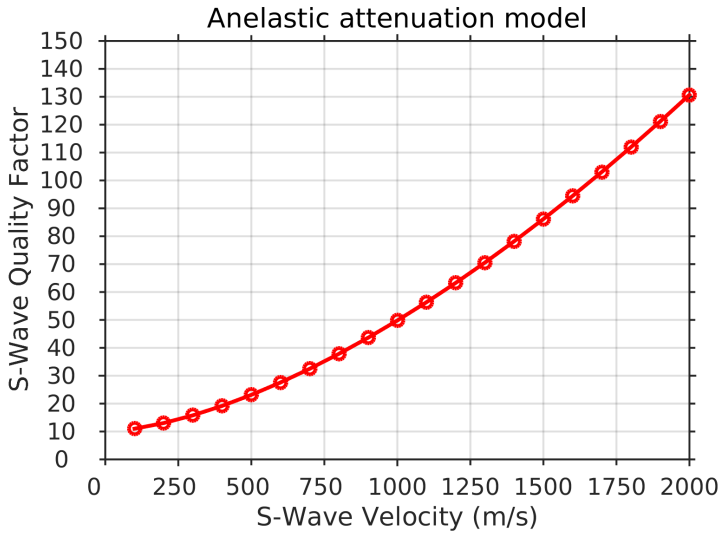

Figure 3.2: Modeled S-wave quality factors from seismic velocity using the simple relation in equation 3.2.

In the transfer function method, the velocity structure is approximated by a linear system under impulse excitation (Kennett and Kerry, 1979). The transfer function method is very simple and provides satisfactory results in many cases, assuming a sufficient level of knowledge of the model parameters (velocity, density and quality factors) and negligible influence of other phenomena such as $2D/3D$ effects and non-linear seismic response. For this reason we decided to compute anelastic amplification from $SHtf$ in addition to direct observations and empirical modeling to all sites of the investigated databases with available one-dimensional velocity profile.

From the databases, however, no information about quality factor (Qs) is made available. Therefore, we introduced an approximated model to derive quality factors from S-wave velocities, in the form:

$$Qs = \left\{ \frac{Vs}{100} \right\}^{1.6} + 10. \tag{3.2}$$

Such model is based on our experience and, although realistic, it should be regarded as purely qualitative, as the comparison with modeled $SHtf$ amplification function is.

3.4 The Swiss reference conditions

All amplification functions (measured or simulated) need to refer to a common reference rock Vs-profile that should as well correspond to the rock reference for the regional probabilistic seismic hazard assessment. The use of an incorrect reference condition may lead to over- or underestimation of the final computed seismic hazard.

All amplification functions (Fourier and response spectral) as well as uniform hazard spectra used in this study are referenced to the national Swiss rock reference conditions (Poggi et al., 2011) in term of average amplification level and anelastic attenuation (attenuation for the reference has been defined as $0.016s$ from the Vs-κ model developed by Edwards and Fäh (2013b));

Chapter 4

Response Spectral Amplification

4.1 Modeling amplification using RVT

Transforming Fourier amplification functions into response spectral amplification functions is a non-linear process. The final result depends, other than on the input amplification model, on the definition of a reference ground motion and the corresponding waveforms used for the calculation. In general, a large number of different waveforms are used to produce mean spectra representative of a specific scenario. However, to analyze multiple magnitude and distance combinations, the use of observed waveforms is impractical, mostly due to the limited availability of empirical data.

To overcome this problem, a stochastic approach based on random vibration theory (RVT, Cartwright and Longuet-Higgins (1956)) can be used to generate "average" response spectral estimates. The method, proposed by Boore (2003), is based on the analytical modeling of the input earthquake spectrum by considering source, path and site characteristics. From that, the corresponding *expected* (in mathematical sense) response spectrum is directly computed using the RVT. This modeling approach however requires the calibration of several parameters which are model (e.g. attenuation, duration) and scenario (e.g. magnitude, distance, stress drop) specific.

To define the reference ground motion of the stochastic modeling we used the parameters of the Swiss spectral model as prescribed by Edwards and Fäh (2013a) for the alpine region. This is also necessary for consistency with the procedure used to retrieve input empirical Fourier amplification models (see the previous chapter) and to preserve the referencing to the Swiss reference rock profile (Poggi et al., 2011).

The procedure to compute response spectral amplification functions using stochastic modeling is then two steps. At first, two response spectra are computed with RVT

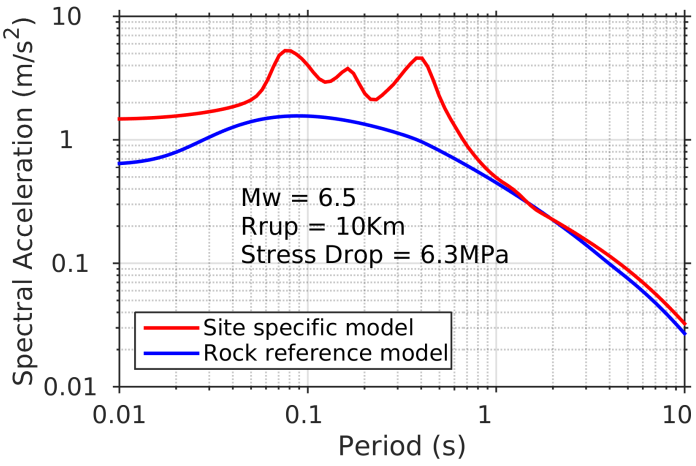

Figure 4.1: Example of acceleration response spectra obtained from spectral modeling (using Swiss specific parametrization) and random vibration theory (RVT).

for a given scenario: the first one including the site specific amplification (target spectrum) while the second not (the rock reference ground motion). Subsequently, the site-specific spectrum is divided by the rock reference spectrum, to isolate the site component in the response spectral domain. It has to be noted that this procedure is essential, as the Fourier and response spectral amplifications (although very similar) are not equivalent. More detail on the method can be found in (Edwards and Fäh, 2013a).

As major drawback of the method, it is sensitive to some parameters having large uncertainty, such as the duration model. In this study we use the Swiss duration model proposed by Edwards and Fäh (2013b), which relates the duration of the ground motion to magnitude and distance. However, this model is calibrated on small magnitudes and might introduce some bias in the computation of response spectral amplitudes when used with large magnitudes (> 5).

4.2 Horizontal to vertical conversion

Response spectral amplification functions for the vertical component are generally not computed directly but derived from the horizontal models by applying a frequency dependent H/V conversion factor. This approach is largely used in

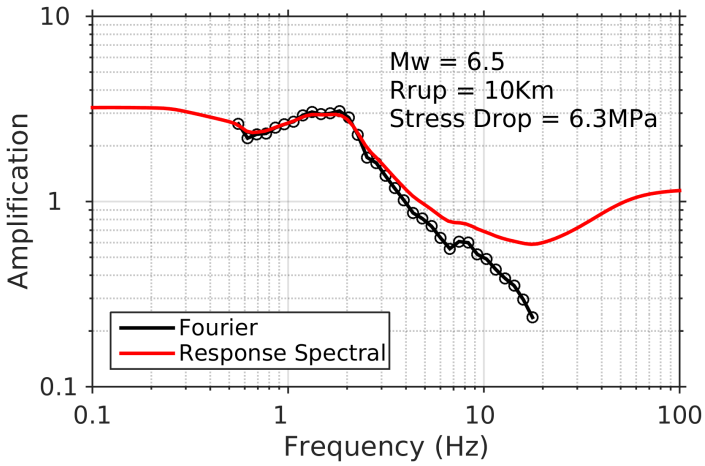

Figure 4.2: Example of the difference between Fourier and response spectral amplification. The two curves show the typical divergence at high frequency.

literature, and it has the advantage to avoid calibrating two separate models for the two components. More importantly, it allows the use of a unique deaggregation scenario consistent between the horizontal and the vertical direction of motion.

To perform the conversion we use two different approaches. The first approach is based on the use of a functional V/H relation to convert directly response spectral ordinates. The functional relation is site-dependent and requires the knowledge of the velocity structure of the site, represented by means of the so called quarter-wavelength parameters (average velocity and impedance contrast). More details on the study can be found in (Poggi et al., 2012a). The method has been calibrated on soft sediment sites, but as it was shown in (Poggi et al., 2012a), it provides consistent results also in case of stiff soil and rock sites.

Conversely, the second approach uses direct V/H spectral ratio observations to correct the Fourier amplification functions $before$ the conversion to response spectral ordinates. Being this method based on site-specific observations, it is supposed to generate a lower uncertainty in the prediction, but on the opposite it has the disadvantage of being applicable only to a restricted number of sites with sufficient recordings. In this case, the empirical V/H spectral ratios are averaged on events of different magnitude and distance (depending on the availability of data). This can introduce some additional bias to the prediction, although quite small.

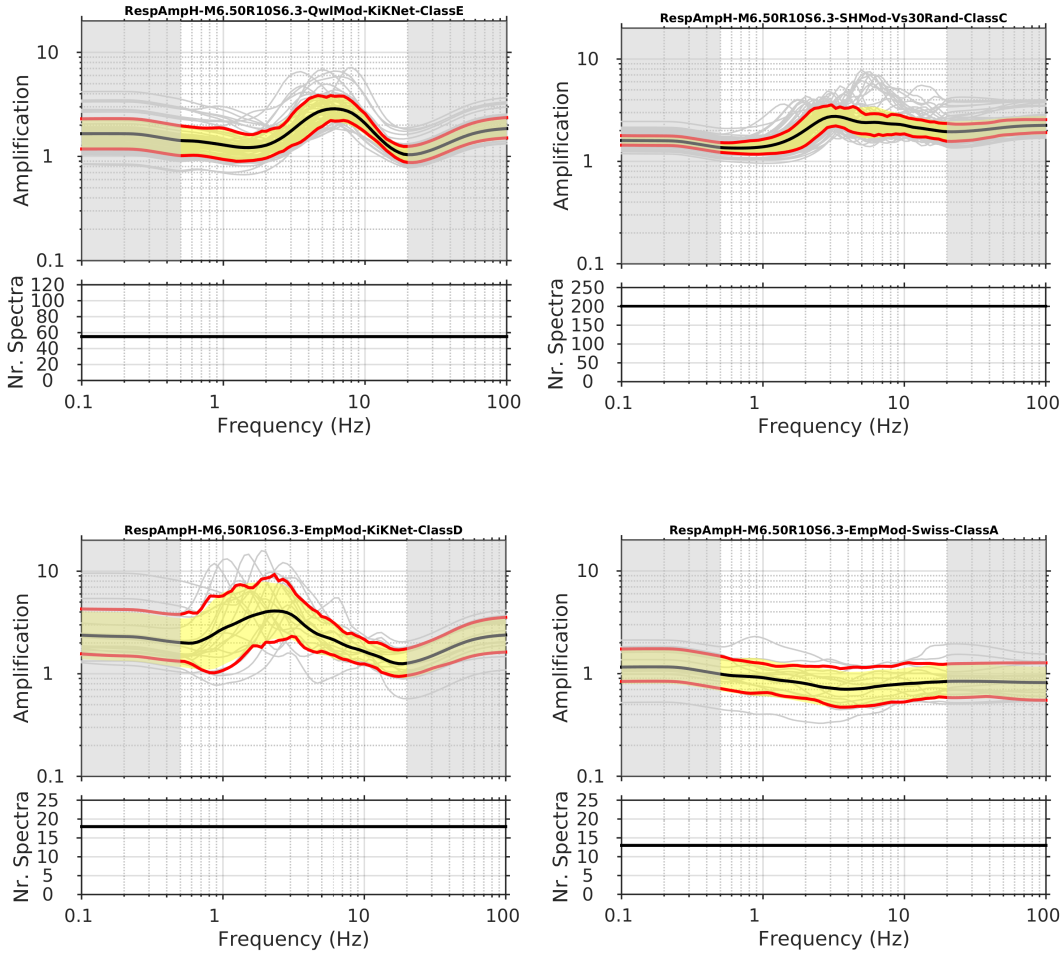

Figure 4.3: Examples of mean response amplification models for different classes, datasets and modeling schemes. The yellow band indicates the region within on standard deviation (in log-statistic), while in red are the 16^th and 84^th percentiles. Gray areas define frequency bands not directly constrained by site amplification data. The title strings on each plot define the specific scenario, modeling approach, dataset and class used for the example (see the README of the electronic data supplement for a comprehensive description of the different title strings).

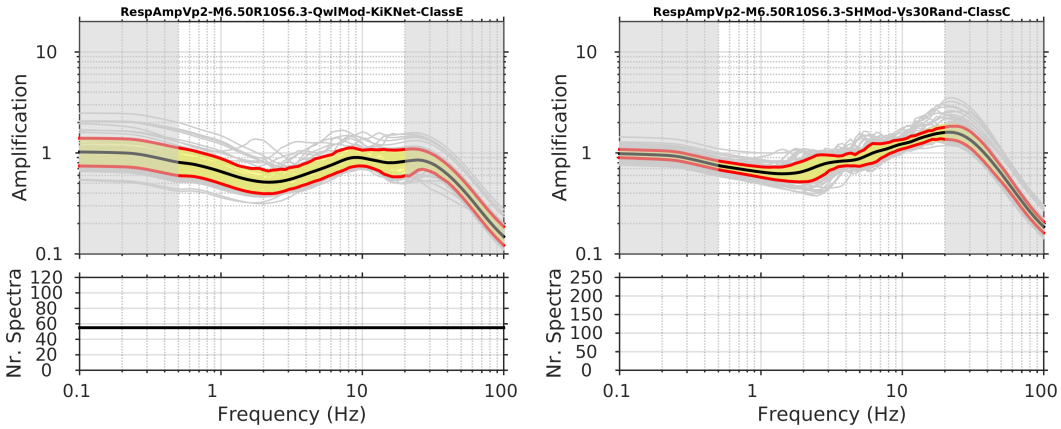

Figure 4.4: Converting the horizontal response spectral amplification functions of figure 4.3 to vertical direction using the quarter-wavelength V/H conversion model (color-code as for figure 4.3).

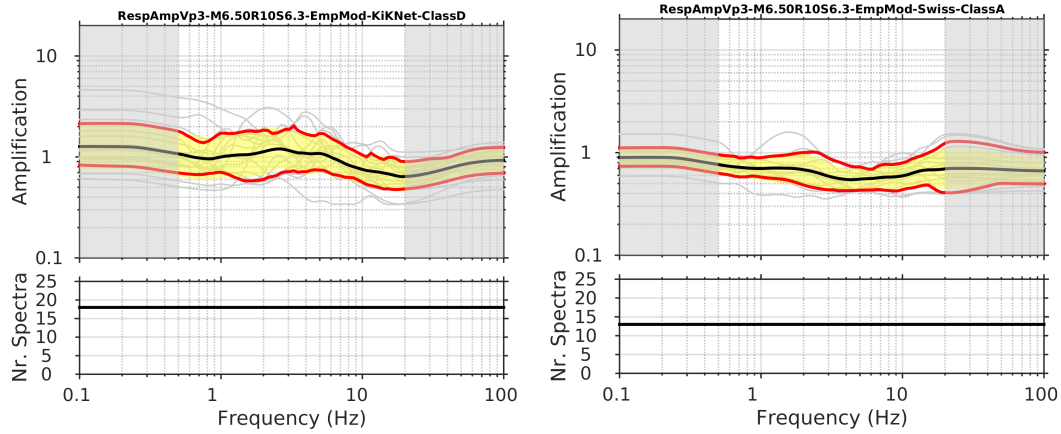

Figure 4.5: Converting the horizontal response spectral amplification functions of figure 4.3 to vertical direction using observed V/H spectral ratios (color-code as for figure 4.3).

4.3 Comparing SIA classes

Response spectral amplifications have been computed for all available sites in each SIA class (A to E), database (Swiss, Japanese and stochastically generated profiles), Fourier amplification type (empirical or modeled with QWL approach and transfer function) and for different combinations of magnitudes (5 to 7 with 0.25 step) and distances ($5Km$ to $25km$ with $5Km$ step). A total of 71275 amplification functions are stored into our database. From those, mean response amplification functions have then been computed for each class separately; a total of 1000 mean curves is available for the analysis (see figure 4.6 for an example computed at $M = 6.5$ and $R_{rup} = 10km$).

By comparing the the different mean curves for each class, the following characteristics are noticeable:

- With the exception of the Swiss empirical observations, all curves show a similar trend and shape, although with generally different amplification levels;
- Average amplification level in each class is progressively increasing from class A to D (as expected);
- The average location of the fundamental frequency of resonance is moving from from high to low frequencies between class A to D. Amplification at resonance shows also a consistent trend, with amplitude increasing with decreasing surface average velocity of the site;
- Class A has generally amplification lower than 1. This is due to the proper referencing to the Swiss rock reference profile, which has $Vs30$ lower than many sites in this class; also the very large amplifications at soft sediment classes C and D are due to the referencing;
- Class E represent the most extreme case, being an intermediate stiff soil or rock site, but with a significant resonance amplification at high frequencies. Class E is not represented in the empirical Swiss database but might deserve further investigation;
- The dissimilarity of the Swiss empirical dataset is mostly due to a lack of calibration data (e.g. in class D) and to the fact that some classes are not fully represented by the available stations. The larger difference stays in the attenuation level, which is quite low if compared to Japan sites.

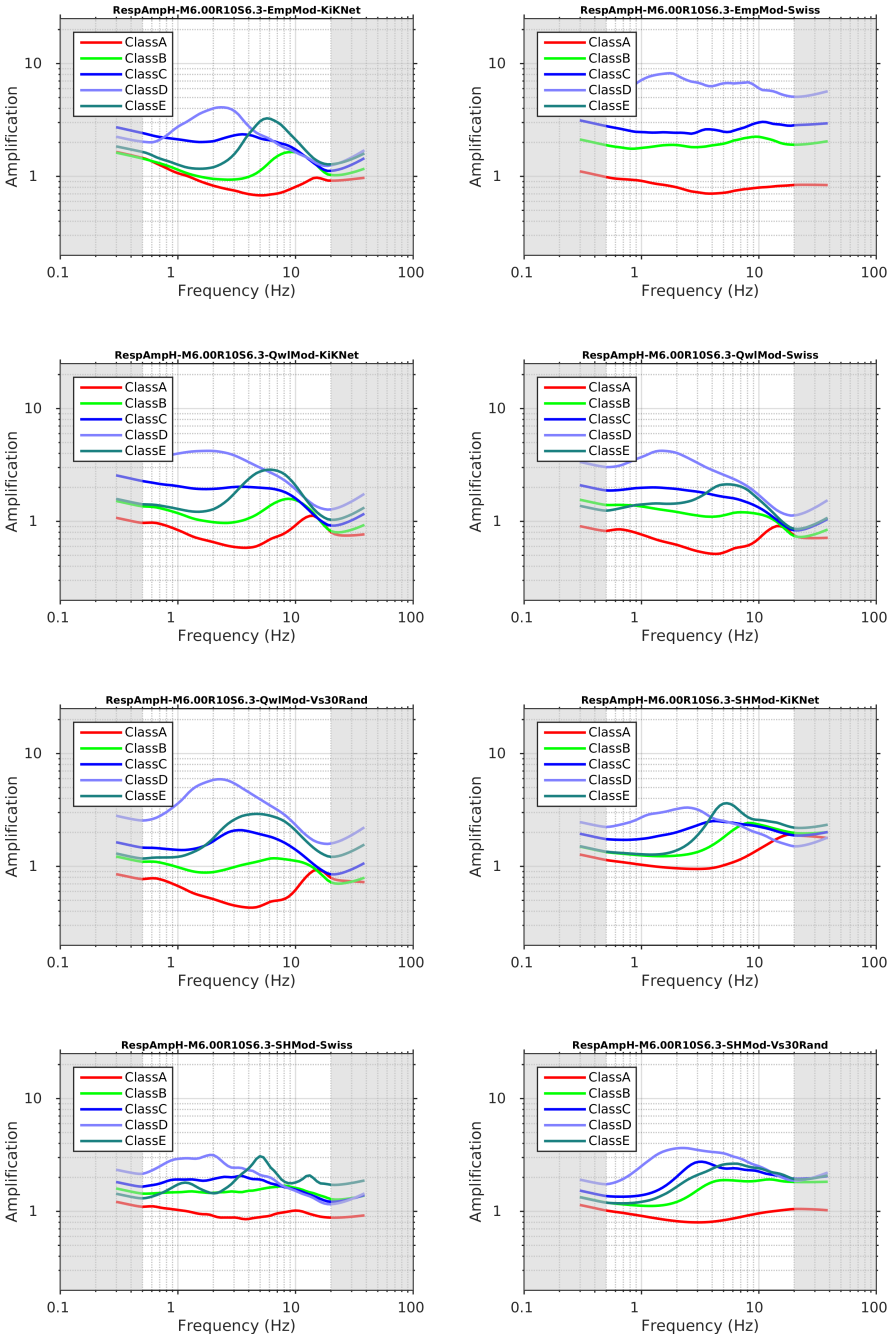

Figure 4.6: Comparison of class-specific mean response spectral amplification curves (horizontal component) for different datasets and modeling methods and for a given scenario of $M = 6.5$ and $R_{rup} = 10km$

Chapter 5

Seismic Hazard Input

5.1 The Swiss seismic hazard 2015

The Swiss Seismological Service provides national support for the implementation, maintenance and dissemination of the probabilistic seismic hazard model for Switzerland. In the present study we used the most recent results from the 2015 revision (Wiemer et al., 2014) of the national model last issued in 2004 (Giardini et al. (2004)). Note that, at the time of this report, the 2015 Swiss Hazard Model is still undergoing a review process and the information presented herein are subject to changes.

In this study we use as reference for the calculation the uniform hazard spectra (UHS) in ground acceleration for four significant return periods: 500, 1000, 5000 and 10000 years (corresponding respectively to the probability of exceedance of 10%, 5%, 1%, 0.5% in a 50 years observation time). The curves were calculated specifically for Sion, considered representative of the hazard scenario in Switzerland (figure 5.1A) in zone 3b.

For the implementation of the elastic design spectra, uniform hazard curves for all periods have been normalized to PGA (assumed as the spectral acceleration at $0.01s$) and then compared. As expected, all curves are very similar in shape, progressively diverging at long periods by a maximum factor of about two. As it will be explained in the next chapter, this variability has been taken into account for the definition of the long period design spectral ordinates.

5.2 Deaggregation scenario: Sion

To identify the most significant magnitude-distance contributions to the computed seismic hazard, a deaggregation analysis has been performed for the site of Sion.

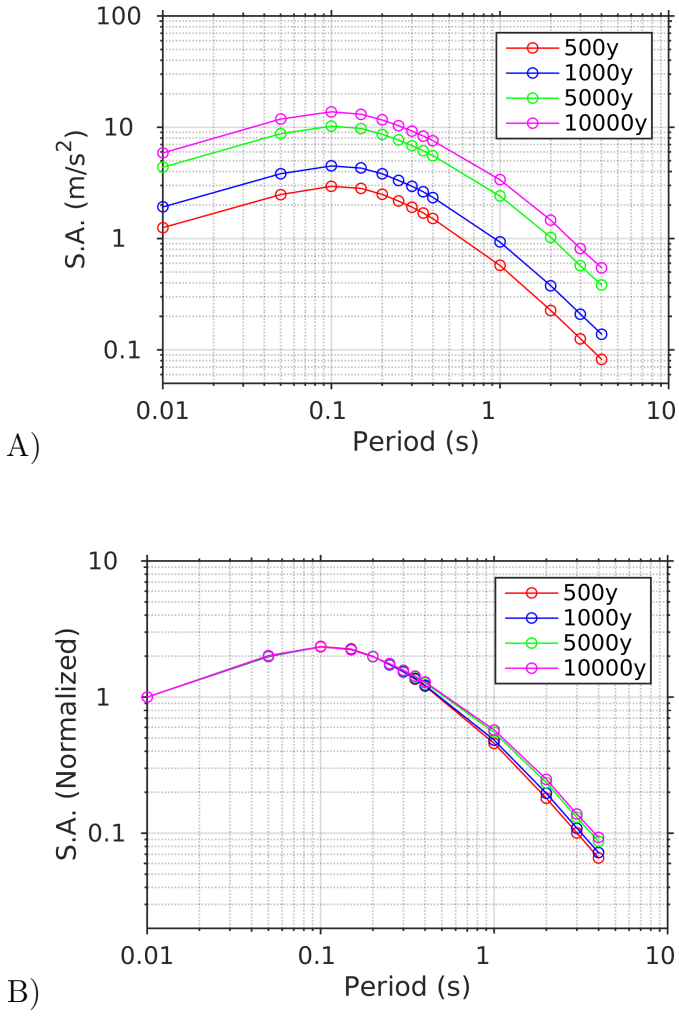

Figure 5.1: Uniform hazard spectra from probabilistic hazard assessment of the Sion site at different return periods. A) Spectral acceleration; B) Normalized spectra to PGA ($0.01s$).

This procedure is essential first of all to restrict the number of magnitude-distance combinations to be included in the subsequent computation of the response spectral amplification functions, but also to avoid the inclusion in the analysis of parameterizations of scarce or no relevance to the total hazard.

The deaggregation of the seismic hazard highlighted some important features (see figure 5.2A). About sensitivity to distance, it is clear that distances below about $20Km$ are the most relevant to the hazard. This result is not surprising and it is also consistent with the results from the 2004 computation (figure 5.2B). Conversely, significant magnitudes for the 2015 hazard are slightly larger than in the 2004 model, especially for the very close distances. Although this result deserve further investigations, a reasonable explanation is given in relation to the different source-depth distribution between the two models. For our purposes, we therefore consider particularly relevant the range of magnitude between 5 and 6.5 and distances between about $5km$ and $20km$. To add conservatism to the analysis, however, we allowed the inclusion in our computations of magnitudes up to 7 and distances up to $25Km$.

5.3 Sensitivity to magnitude-distance

After having selected the range of magnitude and distance of interest from the deaggregation scenario of Sion, we proceeded by testing the sensitivity of these M-R combinations to the computed response spectral amplification functions. By comparing results from the different strategies (observed and modeled spectra), datasets (Swiss and Japanese) and soil classes (see e.g. figure 5.3 and 5.4 for an example from the Japanese empirical dataset) it was evident a minor influence of the magnitude and distance selection to the variability of site response. Such result was expected, but a formal validation was nevertheless needed. More in detail, it was possible to observe that magnitude has a (relatively) larger influence at the low frequencies (short periods), while distance shows more sensitivity to the high frequency region of the amplification spectrum. Softer classes, moreover, show a more pronounced variability, although quite minimal if compared to the total uncertainty of the spectral functions (see previous chapter). Given these results, it was decided to use a unique combination of magnitude ($M = 6.5$) and distance ($R_{Rup} = 10Km$) for the subsequent analyses. The small variability induced by M-R is nevertheless accounted by adding a reasoned conservatism to the final elastic design spectra at appropriate periods.

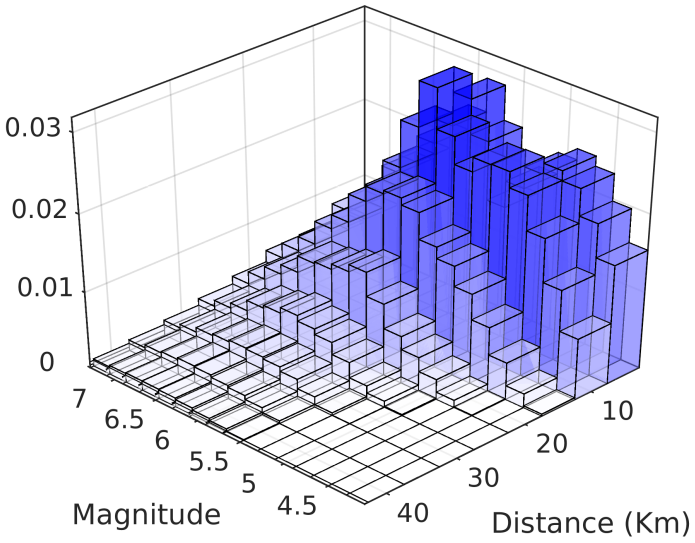

A)

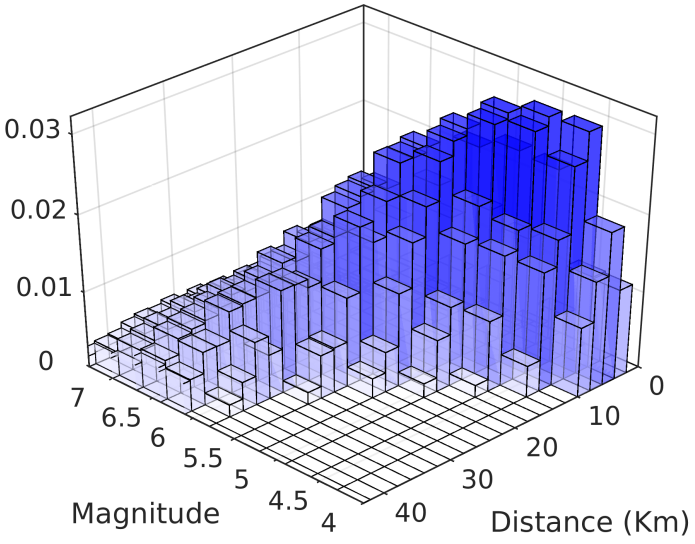

B)

Figure 5.2: Comparison between magnitude-distance deaggregation scenario at PGA for Sion from the 2015 (A) and the 2004 (B) Swiss probabilistic hazard models at $5s$ (in this example for a return period of 500 years).

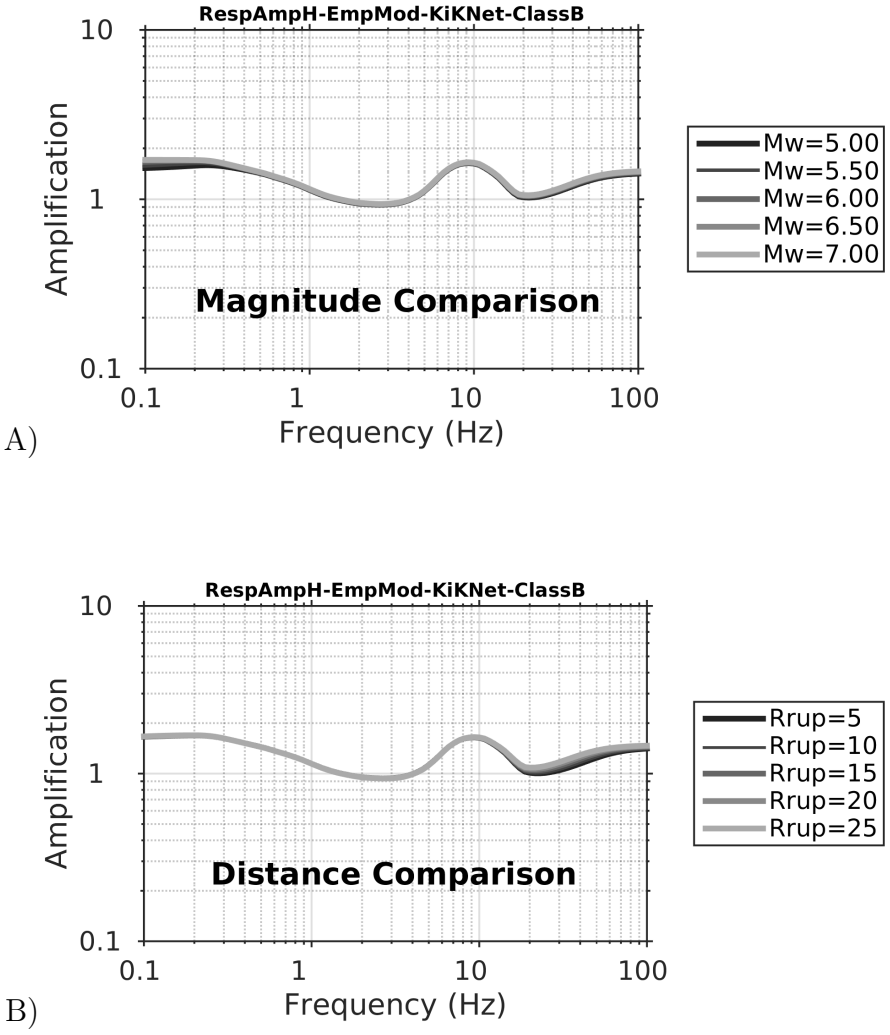

Figure 5.3: Example of sensitivity of response spectral amplification functions (Japanese dataset, *ClassB*) with respect to magnitude (A) and distance (B) according to scenario defined in section 5.2.

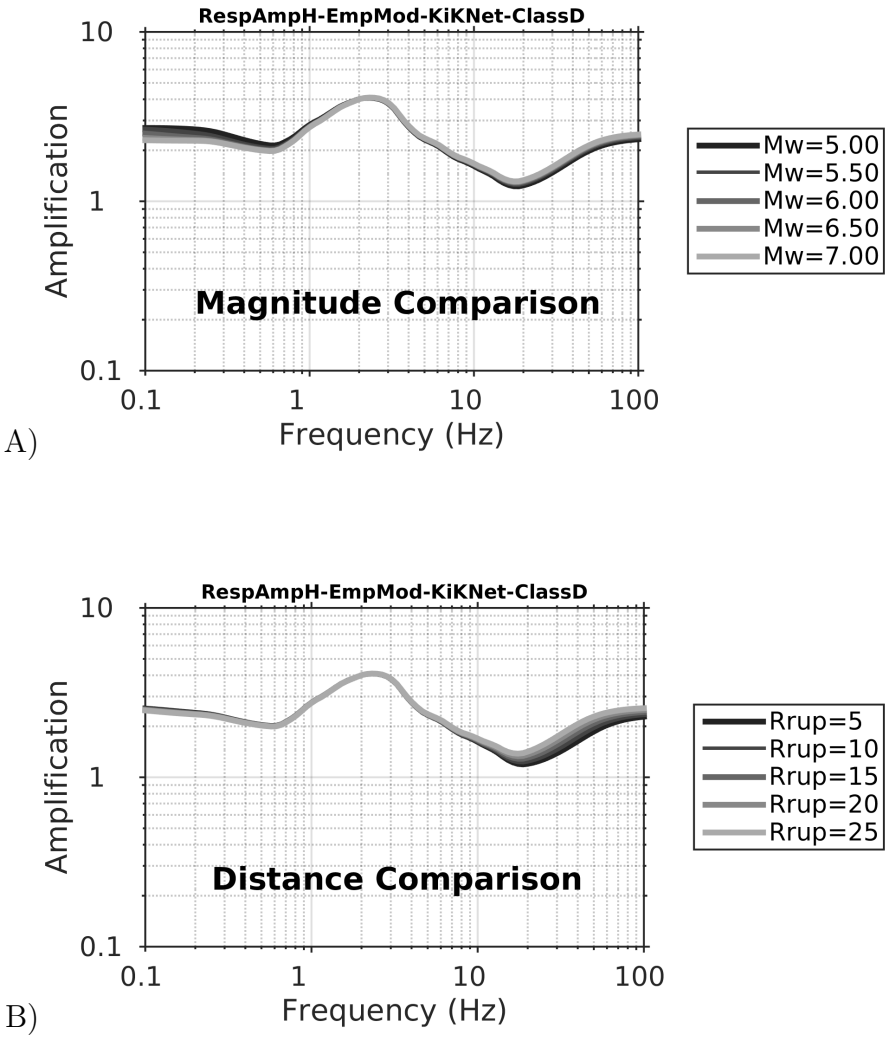

Figure 5.4: Example of sensitivity of response spectral amplification functions (Japanese dataset, *ClassD*) with respect to magnitude (A) and distance (B) according to scenario defined in section 5.2.

Chapter 6

Elastic Design Spectra

6.1 Implementation

Two sets of design spectra has been implemented separately for the horizontal and the vertical direction of motion. The proposed design spectra are based on functional forms used in current normative (SIA261 and Eurocode8). These functional forms are designed to preserve regions of constant ground motion (displacement, velocity and acceleration) and to avoid divergence of the spectra. Moreover, using the original formulation has the additional advantage of an easy comparison of the proposed shapes with those prescribed by existing regulations. Only the values of the control periods (T_B, T_C and T_D) and the plateau spectral acceleration (S) have been modified to accommodate for the variability of the data available in this study. A discussion on the criteria used for implementation is provided in the next section for each class separately. These class-specific spectra are meant to be scaled for the peak spectral acceleration defined for the specific region and return period.

To implement class-specific design spectra, the ensemble of previously obtained site-dependent uniform hazard curves (UHS) was analyzed. Although the curves have been first normalized to the PGA, the variability of the UHS for the different return periods (RP) is nevertheless accounted in the implementation of the design spectra by adding sufficient conservatism to the design at long periods (a detailed discussion on the variability of hazard curves at different return periods is given in chapter 5). Is to be noted that normalized design spectra are asymptotic to the class-specific S values only at period $0s$; the S value is not necessarily equal to one for all classes (see equation 25 at page 60 of the SIA261 normative), as it is influenced by the site response of the class.

Moreover, given the small sensitivity of the response spectral amplification functions to magnitude and distance pairs which are relevant for the deaggregation scenario, a unique combination of magnitude and distance ($M = 6.5$ and $R = 10Km$) has been used for the definition of the design shapes.

6.2 Horizontal design spectrum

To fit the design spectral shapes to the site-dependent spectral acceleration curves, we used a logic-tree approach, providing different significance to the different amplification models according to representativeness of each model to the (expected) mean ground motion level for each class. As previously introduced, observed amplification functions for Switzerland have a rather high amplification level for those SIA classes corresponding to soft sediment sites. This is due to the location of these stations within the Swiss strong motions network. In many cases the observed ground motion is affected by phenomena such as geometrical effects, 2D/3D resonances and edge generated surface waves which introduce significant amplification (e.g. in case of deeply incised alpine valleys, see Michel et al. (2014)).

The different (normalized) spectral acceleration curves for each tested amplification model are presented in figure 6.1 for the $500y$ return period and in figure 6.2 for the $10000y$ return period. In green are the empirical observations (Switzerland and Japan); in yellow the analytical amplification from SH-wave transfer function; in black the quarter-wavelength amplification models for Switzerland and Japan, while in blue the amplification models from the same model but from stochastically generated velocity profiles (dashed and dotted lines for respectively plus one and two standard deviations, to provide a first order indication of the model variability).

To fit the design spectrum, several criteria were considered, beyond the simple enveloping of the available curves. In the long periods we accounted for the effect of different return periods on the hazard. In this region, the design shape is consistently above the different site-dependent models. As well, the control periods T_D is imposed to be equal to $2s$ for all classes.

With respect to the elastic acceleration design spectra from current SIA normative (see figure 6.3) the proposed shapes have generally higher amplitudes of the plateau (below about $0.5 - 0.6s$) for all classes, with the exception of class A. These large amplitudes are related to the development to resonance phenomena in sediment sites (stiff and soft), which are dominant in the intermediate-to-high frequency range of the site amplification functions. Conversely, the proposed model has a design amplitude lower than what prescribed by the SIA normative for long periods. Its shape is in this range more similar to the *type*2 spectra of the Eurocode.

The values for the control periods and plateau acceleration for the horizontal component are presented in table 6.1.

$Class$	S	T_B $[s]$	T_C $[s]$	T_D $[s]$
A	1.00	0.06	0.25	2.00
B	1.80	0.08	0.20	2.00
C	2.00	0.10	0.25	2.00
D	3.00	0.15	0.35	2.00
E	2.60	0.12	0.20	2.00

Table 6.1: Values of the parameters needed to define the elastic design spectrum proposed in this study (horizontal component).

$Class$	S	T_B $[s]$	T_C $[s]$	T_D $[s]$
A	0.65	0.06	0.25	2.00
B	0.80	0.06	0.25	2.00
C	1.00	0.07	0.25	2.00
D	1.60	0.10	0.30	2.00
E	1.15	0.08	0.20	2.00

Table 6.2: Values of the parameters needed to define the elastic design spectrum proposed in this study (vertical component).

6.3 Vertical design spectrum

For the definition of the elastic design response spectra for the vertical component, we first applied the approach prescribed by the SIA normative, which consists in reducing the shape of the horizontal component by a factor of 0.7. Although this approach provides a design shape quite conservative with respect to the vertical models, in some periods the amplitudes are largely overestimated. We therefore proceeded also with the implementation of separate design spectrum by defining a new set of control parameters. The values for the control periods and plateau acceleration for the vertical component are presented in table 6.2.

The selection criteria were similar to those used for the horizontal component (figure 6.5), with the additional constraint of keeping the design of the horizontal and vertical shapes as consistent and comparable as possible (figure 6.6). In mode detail, the vertical design spectrum for class A is in agreement with the one obtained by scaling the horizontal component. For all other classes, however, the newly proposed

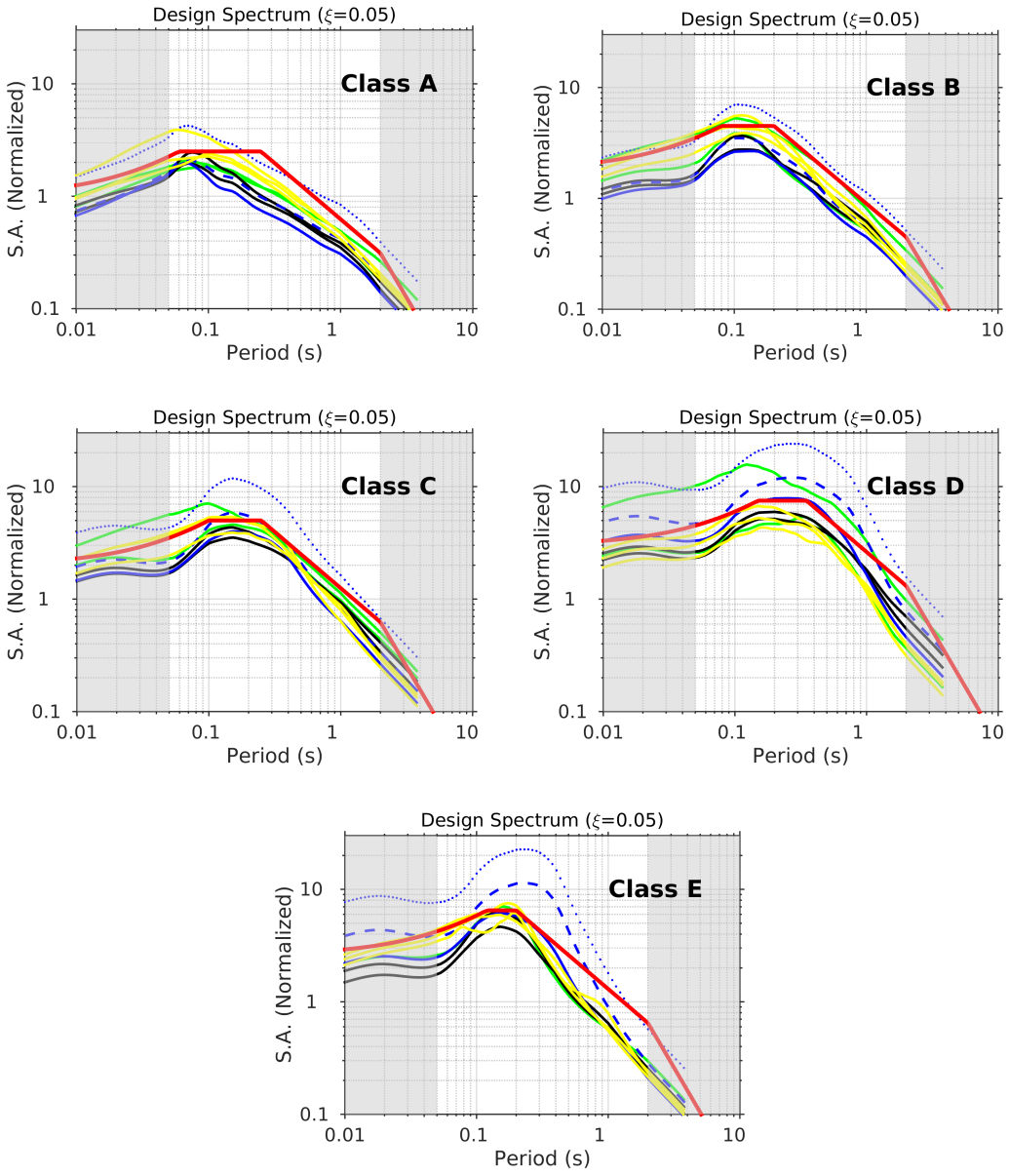

Figure 6.1: Normalized spectral acceleration curves for the different SIA class (horizontal component). Different colors represent different approaches to compute amplification (see text for a complete description). Proposed design spectra is in red. Gray areas represent the regions where amplification models are poorly constrained by actual data. The UHS for 500 years return period was used.

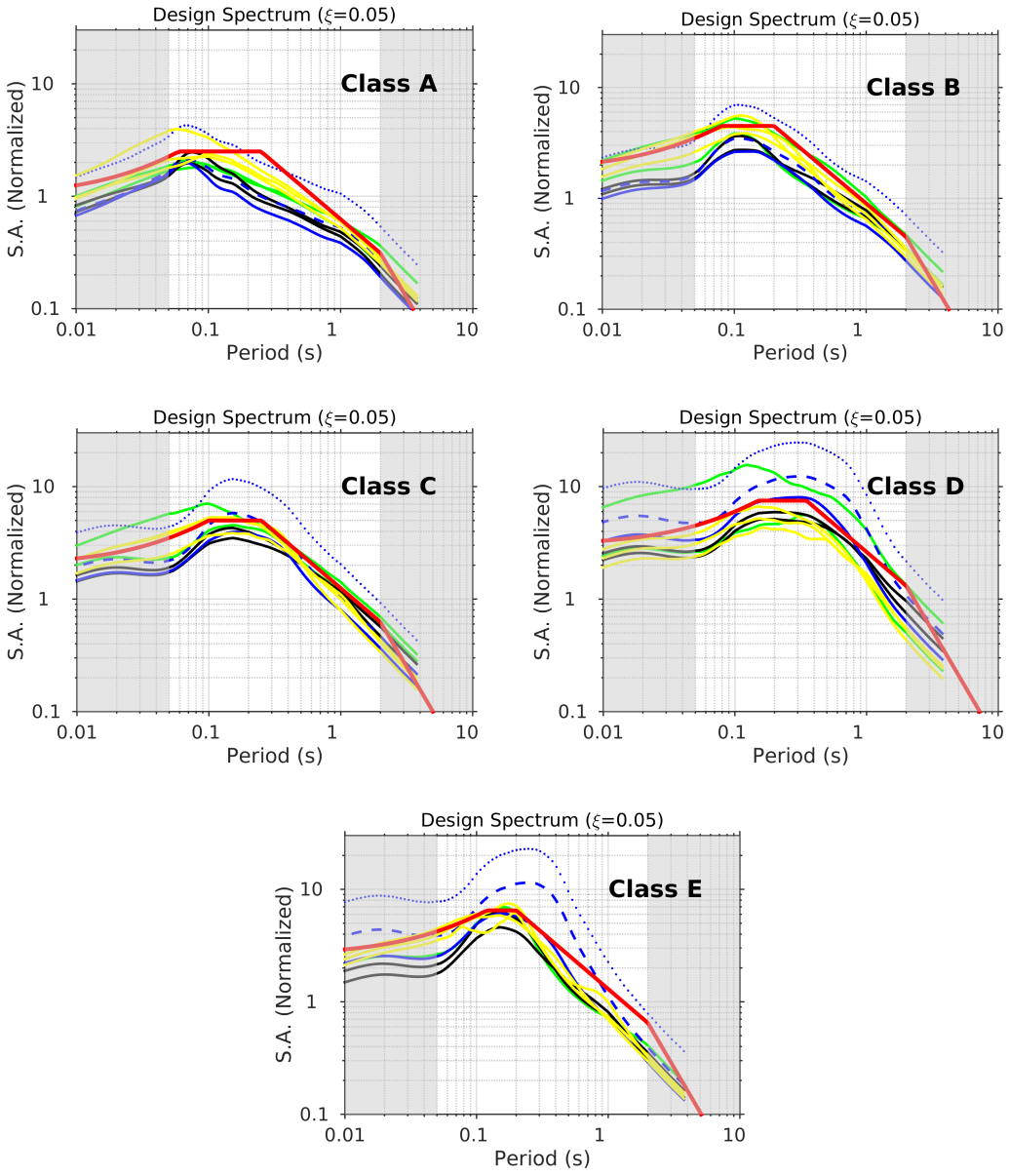

Figure 6.2: Normalized spectral acceleration curves for the different SIA class (horizontal component). Different colors represent different approaches to compute amplification (see text for a complete description). Proposed design spectra is in red. Gray areas represent the regions where amplification models are poorly constrained by actual data. The UHS for 10000 years return period was used.

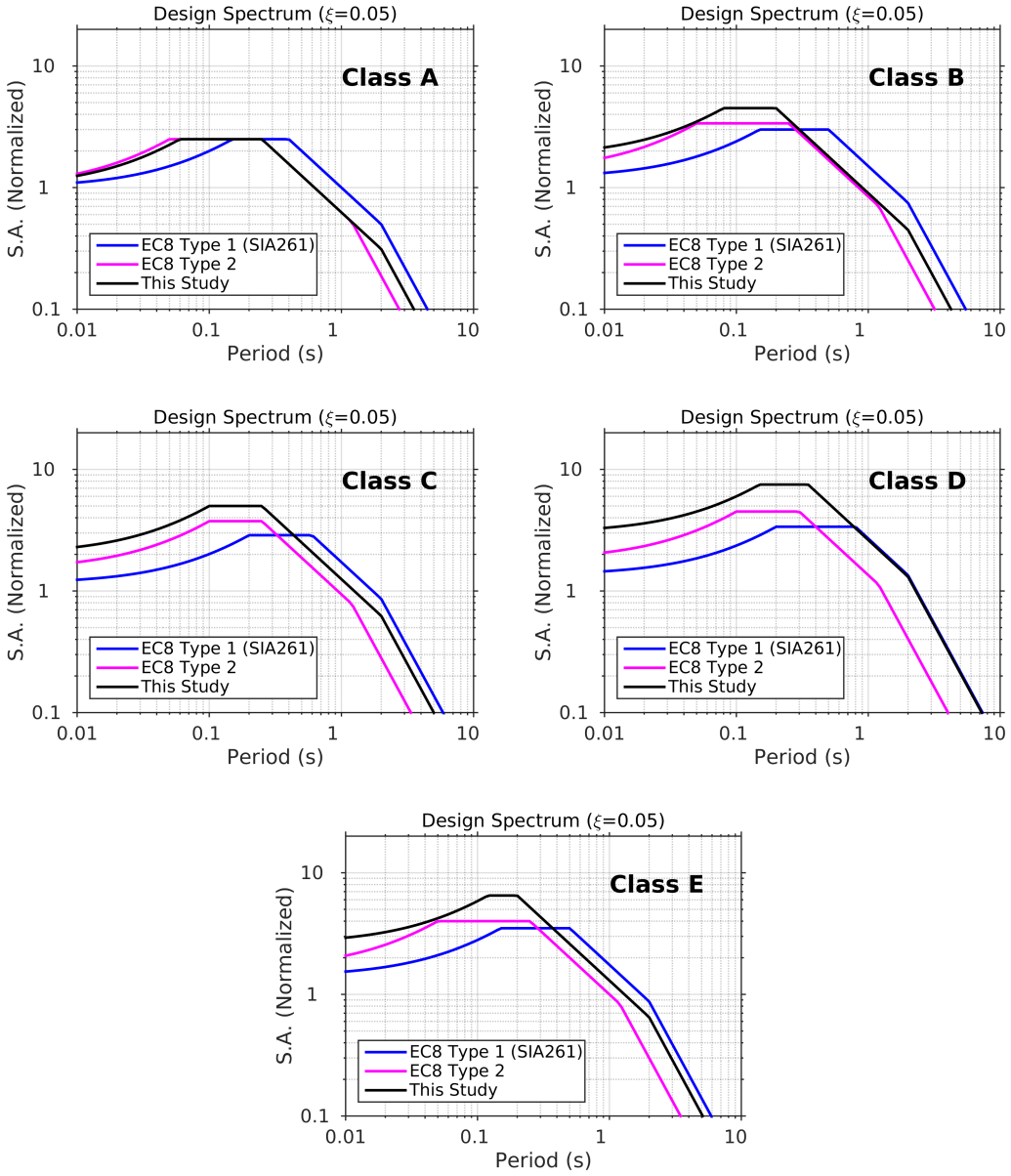

Figure 6.3: Comparison between the proposed normalized design spectra for the horizontal component and the design spectra from current normative (SIA and Eurocode).

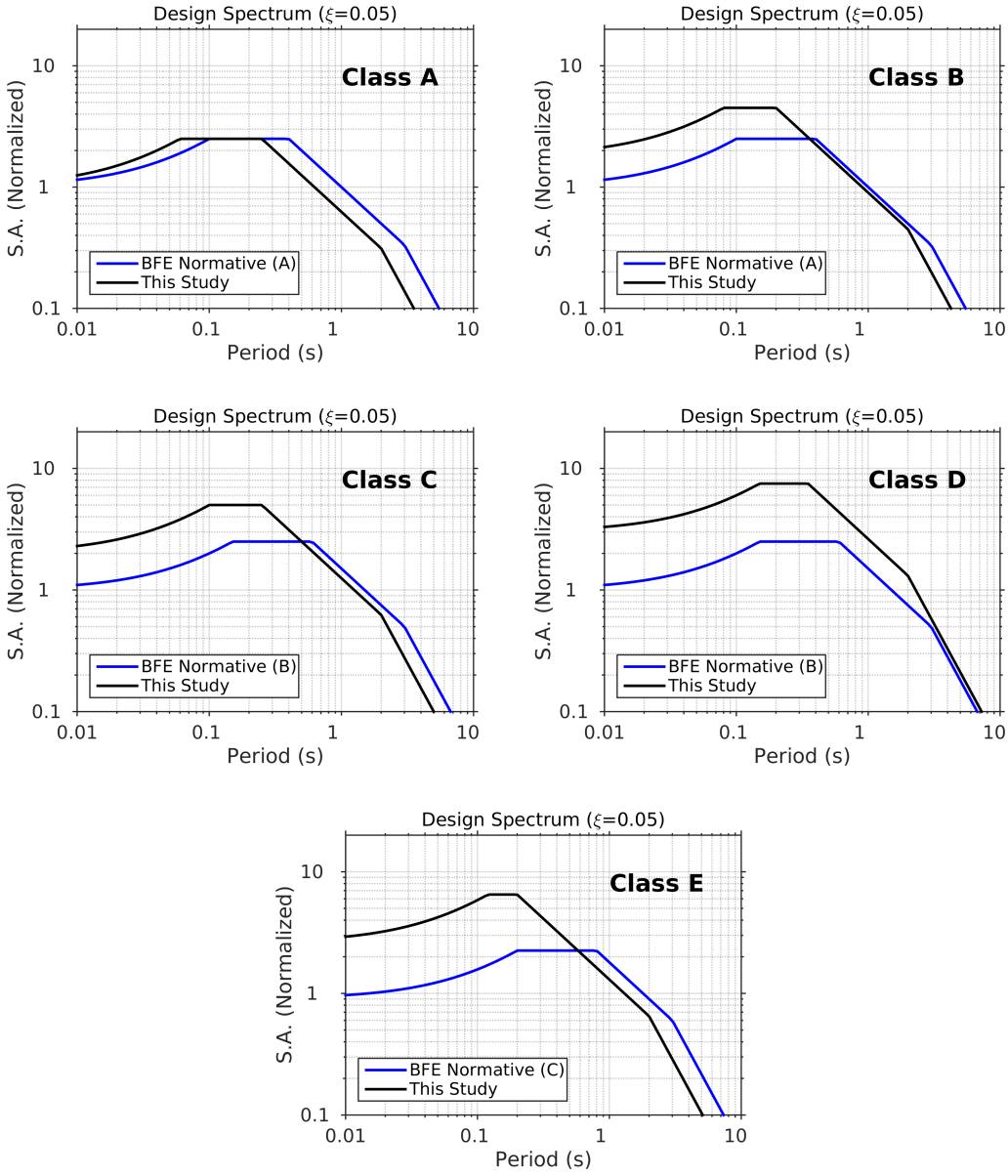

Figure 6.4: Comparison between the proposed normalized design spectra for the horizontal component and the design spectra from current BFE normative.

shapes are always below their scaled counterpart. The value of 0.7 appears therefore to be too conservative for sediment classes, as the vertical component is likely not affected by resonance phenomena as significant as for the horizontal.

Moreover, by comparing the proposed design spectrum with the other normative spectra (horizontal shape scaled by the factor 0.7) it is possible to observe an overall agreement of our model with the *type*2 spectra from Eurocode (figure 6.7). The agreement is for both the long-period flank amplitudes and particularly for the plateau level. This observation gave us additional evidence that *type*2 spectral model could be to a certain extend better representative of the Swiss conditions, with particular regards to the short periods.

6.4 Damping scaling

The SIA and Eurocode normatives prescribe a simple approach to account for different damping conditions. Such approach consists in applying a scaling factor η function of the damping ξ as defined in the equation:

$$\eta = \sqrt{\frac{1}{0.5 + 10\xi}} \tag{6.1}$$

We tested the applicability of this approach by investigating different damping scaling factors available from literature. We have examined in particular the approaches proposed by (Rezaeian et al., 2014) and (Akkar et al., 2014); although the two methods provide quite comparable results for the horizontal component, in this study we decided to adopt the first approach, which was calibrated on the NGA $West2$ database.

In the article Rezaeian provides a functional form to compute magnitude-distance dependent scaling factors as a function of the input damping ratio in percentage. An example of these correction factors versus period is given in figure 6.8 for the values of 2%, 4%, 5%, 10%, 15%. These factors are then applied to the response spectra amplification functions (e.g. figure 6.9). As visible from these example, such correction is period-dependent: asymptotic to value one at PGA, with maximum at intermediate periods, around about $0.2 - 0.4s$, and progressively decreasing with increasing period. The actual values of the correction scale effectively with magnitude, but are less sensitive to distance (figure 6.10A). However magnitude

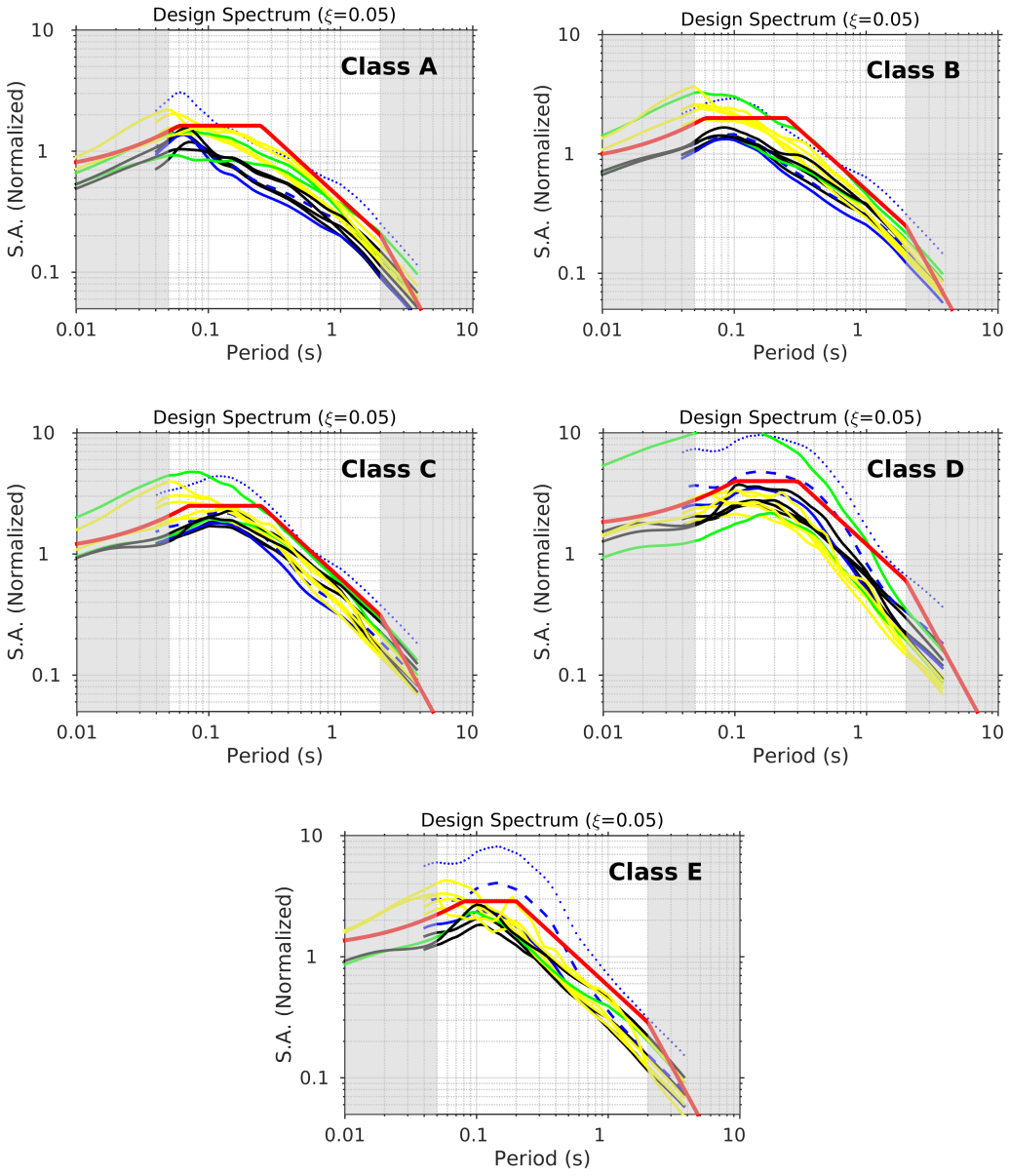

Figure 6.5: Normalized spectral acceleration curves for the different SIA class (vertical component). Different colors represent different approaches to compute amplification (see text for a complete description). The shape of the proposed design spectra is in red. Gray areas represent the regions where amplification models are poorly constrained by actual data.

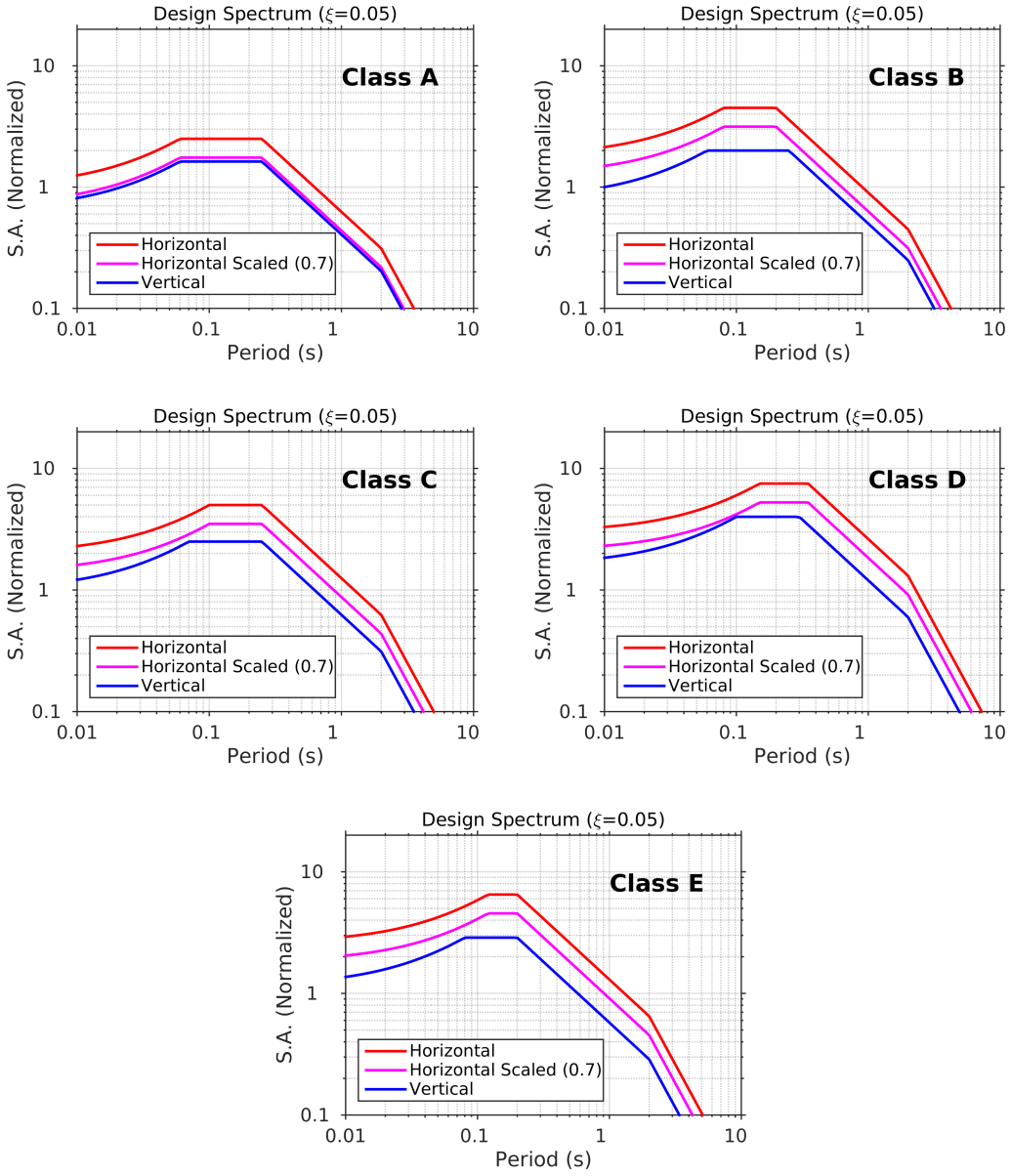

Figure 6.6: Comparison between the proposed design spectra for the horizontal, the horizontal scaled by a factor 0.7 and the vertical component.

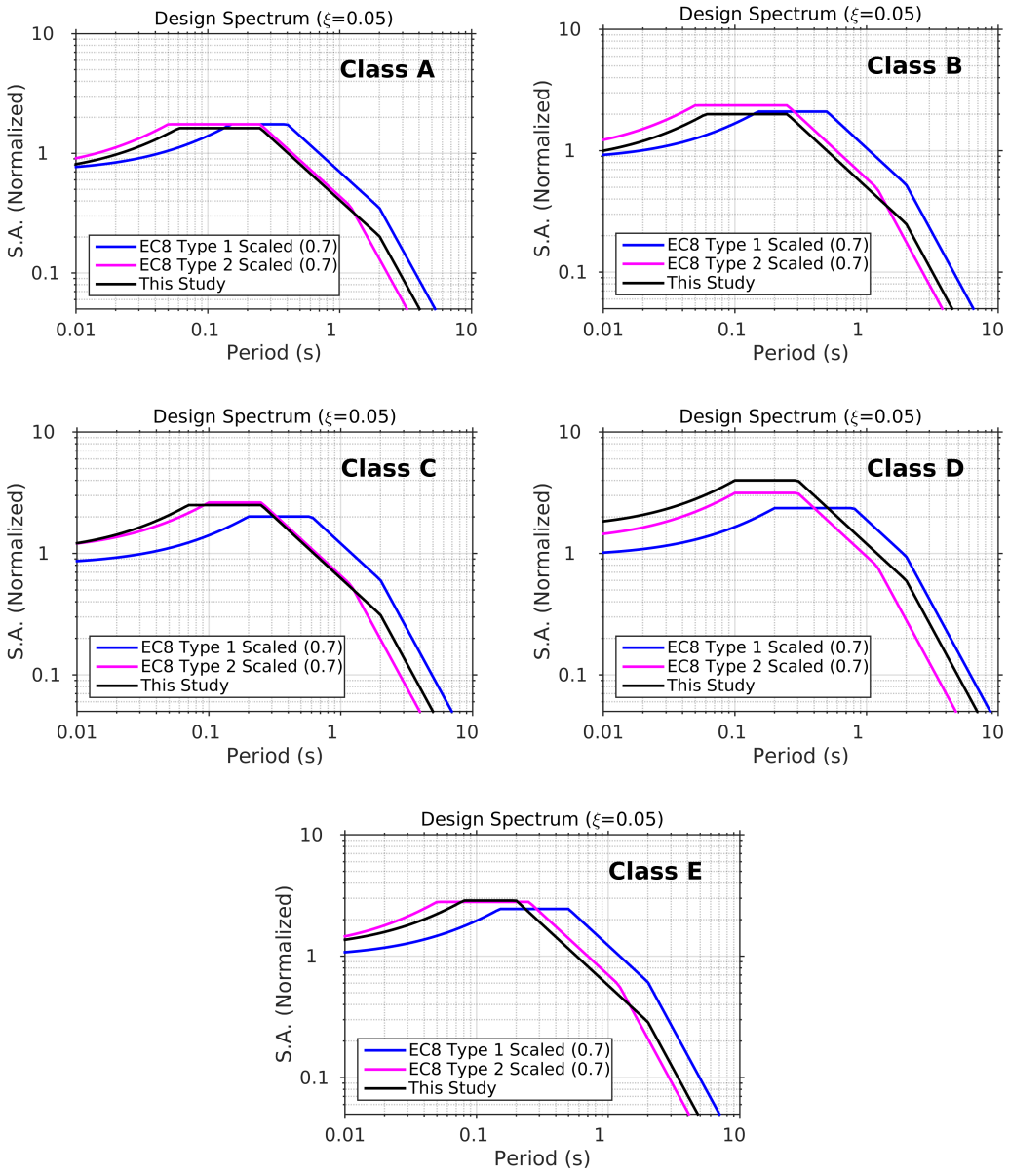

Figure 6.7: Comparison between the proposed normalized design spectra for the vertical component and the horizontal design spectra from current normative (SIA and Eurocode) scaled by a factor of 0.7.

scaling is significant only at long periods (about $> 1s$) but not relevant for the intermediate to small period range (e.g. figure 6.10B).

The scaling prescribed by SIA normative is period and magnitude independent. It is therefore necessary to understand if this correction is calibrated as a mean response or for a given set of period/magnitude. By comparing the actual values prescribed by SIA at selected damping ratios (figure 6.13) with those from Rezaeian, a good matching is found for periods of about $2-3s$ (relevant for structures) and magnitude in the range $6.5-7$ (e.g. figure 6.12), which is consistent with the results from hazard deaggregation reported in the previous chapter.

As a conclusion, the correction factors prescribed by the normative appears to be a meaningful way to scale the design response spectra for damping values different than 5%. A possible extension could be the definition of a scaling procedure to account for different magnitude scenarios at long periods. In figure 6.13 are presented the results of magnitude scaling computed with the following simple form:

$$\gamma = (6.5 - M)(\xi - 0.05) + 1. \tag{6.2}$$

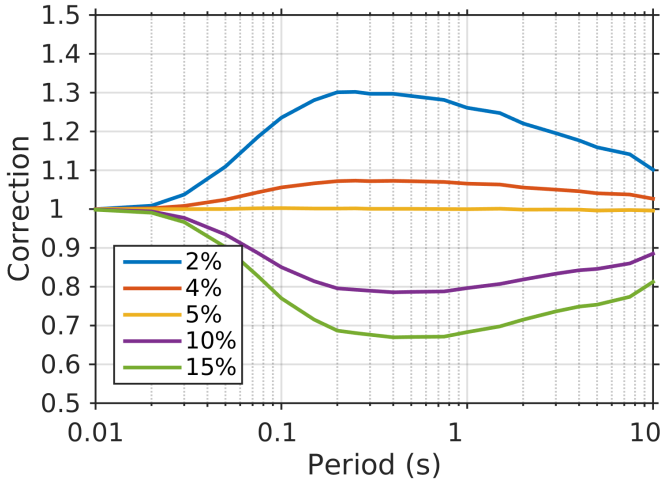

Figure 6.8: Example of response spectral correction functions for different damping values according to Rezaeian et al. (2014). The functions in this example are calculated for a scenario $M = 6.5$ and $R_{Rup} = 10Km$.

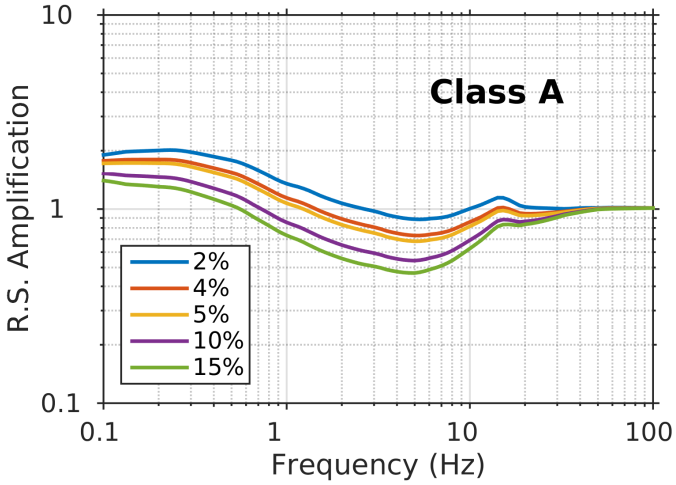

Figure 6.9: Example of application of the correction functions prescibed by Rezaeian et al. (2014) to the mean response spectral amplification for class A of the Swiss empirical dataset.

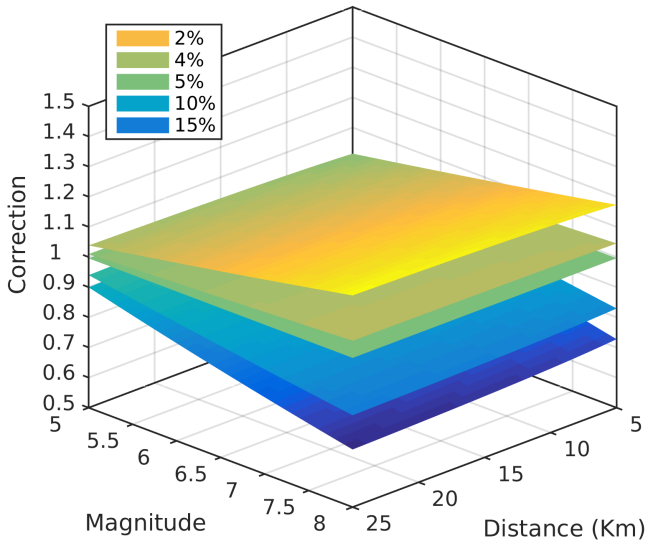

A)

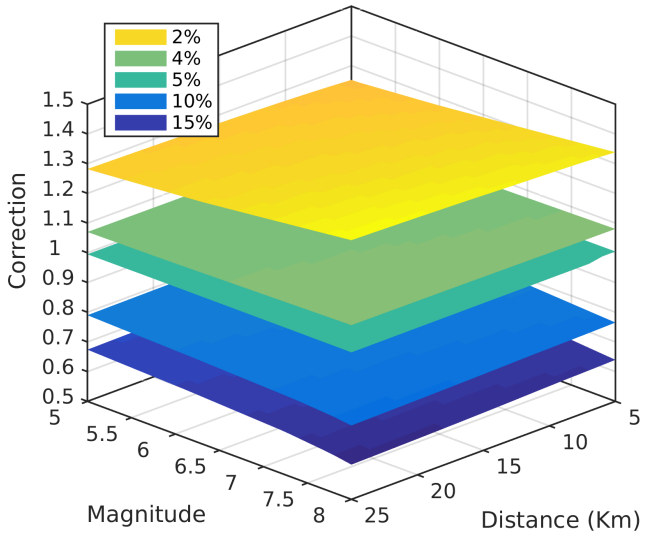

B)

Figure 6.10: Sensitivity of the damping correction factors proposed by Rezaeian et al. (2014) to magnitude and distance at 0.2s (A) and 10s (B).

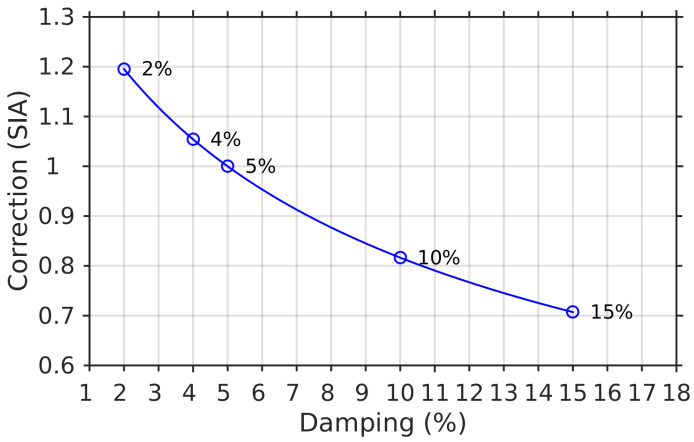

Figure 6.11: Example of damping correction factors as prescribed by SIA normative for some representative damping values.

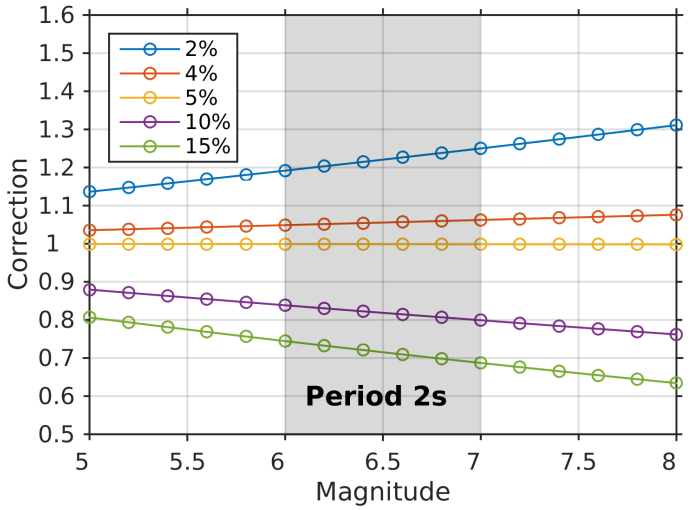

Figure 6.12: Example of damping correction factors versus magnitude as proposed by Rezaeian et al. (2014). This example is calculated for a period of $2s$ and $R_{Rup} = 10Km$.

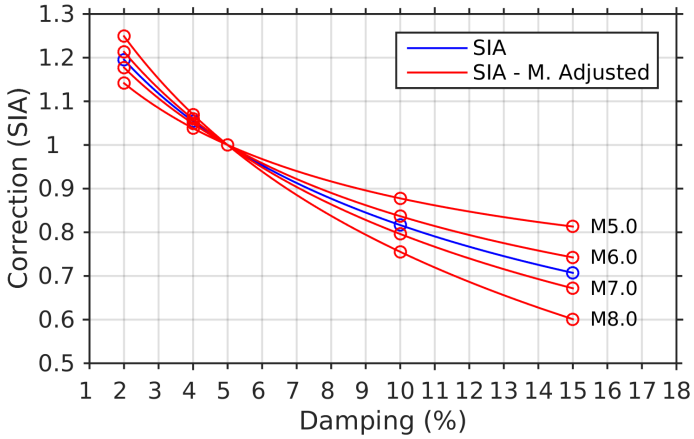

Figure 6.13: Adjusting the damping correction factors from the SIA normative to different magnintude using the equation 6.2.

Chapter 7

Conclusions

Within this study we propose a new set of coefficients for the implementation of soil-class-specific design spectral shapes for both the horizontal and the vertical components. The proposed models have been calibrated on normalized uniform hazard spectra (UHS) from the probabilistic seismic hazard scenario at Sion (Switzerland). To account for the variability of site response in different soil conditions, a set of mean response spectral amplification functions (observed and modeled) was defined for the different soil classes and applied to the UHS.

The proposed design spectral shapes have a functional form consistent with the present normative, but they differ from these in terms of controlling periods (T_B, T_C and T_D) and plateau level (S). By comparing the proposed shapes with current normative spectra, some relevant features are noticeable, which are listed in the following.

For the horizontal component:

- The long period part of the developed acceleration spectrum is generally lower than SIA design spectrum, but always between the shapes of *type*1 (equivalent to SIA) and *type*2 spectra of the Eurocode;
- At intermediate to short periods (high frequency region, where resonance phenomena are relevant in soft sediment sites) the plateau amplitude is consistently above the present normative, and also generally higher than the EC *type*2 spectrum.
- When using the functional form defined in EC8, the large plateau amplitudes have the drawback of imposing an increased acceleration at PGA, which appears to be not realistic. A possible solution would be to use a different equation for the design spectrum at short periods (before T_B) with a steeper amplitude decay. This needs further discussion.

- The conservative choice of a *type*1 spectrum in the present SIA code at long periods might be desirable, also accounting for near-source effects such as source directivity. However at short periods, the *type*1 spectrum is not sufficiently conservative. A combination with a spectrum as proposed in our study or a spectrum similar to EC *type*2 should be discussed.

Regarding the vertical component:

- The recipe prescribed by SIA normative (scaling for a factor 0.7) can be accepted, although it turned out to be a conservative choice for all spectral ordinates. If a reduction of the level of conservatism is targeted, however, the proposed model might be preferred.

Regarding different values for the damping:

- Procedures from SIA and Eurocode were tested to account for different damping. They appeared to be a meaningful way to scale the design response spectra for damping values different than 5%. An adjustment to the magnitudes might be discussed.

Additional issues raised during this study are related to the soil classes defined in the normative. In particular we observed that a classification scheme based on the use of Vs_{30} only is too simplistic. In particular:

- The broadband amplification observable in $Class\ B$ and C is a clear indication that large averaging of resonance amplification effects occurs over different frequency bands. To reduce such variability (and therefore the model uncertainty) a classification scheme that includes *also* the use of the fundamental frequency of resonance of the site (f_0, measured or calculated) might be advisable.
- Some sites might be influenced by special phenomena, such as 2D/3D resonance and edge-generated surface waves, which can increase the amplitude of ground motion by large factors. This is typical the case in Switzerland for deeply incised alpine valleys. Also in this case, the presence of these special effects should be accounted for in the normative, with a corresponding scaling procedure.

- *Class E* is a very special class of difficult identification that is presently not well represented in the data set for Switzerland. The use of the fundamental frequency of resonance of the site (f_0) would also help in this case.

Lastly, some features of our model could be improved with additional scientific research. In particular:

- The duration model developed for Switzerland might not account properly for the effects of very soft sediment sites, where the generation of long period surfaces wave might lead to increased shaking duration. This would also have a direct impact on the amplitude level of the response spectral amplification functions.
- Site attenuation (in term of attenuation parameter κ) is still poorly constrained in many cases; this leads to very large uncertainties in the prediction of high frequency ground-motion amplification. There is a need for new methods for a better estimation of the site attenuation term, either by direct measurement or from the definition of innovative site-specific proxies.

Bibliography

S. Akkar, M.A. Sandıkkaya, and Ay B.Ö. Damping scaling factors for vertical elastic response spectra for shallow crustal earthquakes in active tectonic regions: "average" horizontal component. *Bull. Earthq. Eng.*, 12:517–547, 2014.

S. Aoi, T. Kunugi, and H. Fujiwara. Strong-motion seismograph network operated by nied: K-net and kik-net. *J. Jpn. Assoc. Earthquake Eng.*, 4:65–74, 2004.

D. Boore. Simulation of ground motion using the stochastic method. *Pure and applied Geophysics*, 160:635–676, 2003.

D.E. Cartwright and M.S. Longuet-Higgins. The statistical distribution of the maxima of a random function. *Proc. Roy. Soc. Lond.*, 237:212–232, 1956.

B. Edwards and D. Fäh. A stochastic ground-motion model for switzerland. *Bull. Seism. Soc. Am.*, 103:78–98, 2013a.

B. Edwards and D. Fäh. Measurements of stress parameter and site attenuation from recordings of moderate to large earthquakes in europe and the middle east. *Geophys. J. Int.*, 194:1190–1202, 2013b.

B. Edwards, D. Fäh, and D. Giardini. Attenuation of seismic shear wave energy in switzerland. *Geophys. J. Int.*, 185:967–984, 2011.

D. Giardini, S. Wiemer, D. Fäh, and N. Deichmann. Seismic hazard assessment of switzerland. *Swiss Seismological Service, ETH Zürich*, 2004.

W. B. Joyner, R. E. Warrick, and T. E. Fumal. The effect of quaternary alluvium on strong ground motion in the coyote lake, california, earthquake of 1979. *Bull. Seism. Soc. Am.*, 71:1333–1349, 1981.

B.L.N. Kennett and N.J. Kerry. Seismic waves in a stratified half space. *Geophys. J. R. Astr. Soc.*, 57:557–583, 1979.

C. Michel, B. Edwards, V. Poggi, J. Burjanek, D. Roten, C. Cauzzi, and D. Fäh. Assessment of site effects in alpine regions through systematic site characterization of seismic stations. *Bull. Seism. Soc. Am.*, 104:2809–2826, 2014.

V. Poggi, B. Edwards, and D. Fäh. Derivation of a reference shear-wave velocity model from empirical site amplification. *Bull. Seism. Soc. Am.*, 101:258–274, 2011.

V. Poggi, B. Edwards, and D. Fäh. Characterizing the vertical to horizontal ratio of ground-motion at soft sediment sites. *Bull. Seism. Soc. Am.*, 102:2741–2756, 2012a.

V. Poggi, B. Edwards, and D. Fäh. The quarter-wavelength average velocity: a review of some past and recent application developments. *15th WCEE. Lisbon, Portugal*, 2012b.

V. Poggi, J. Burjanek, B. Edwards, and D. Fäh. Sed extended velocity profiles at rock sites. *PRP Technical report*, SED/PRP/R/039/20130822, 2013a.

V. Poggi, B. Edwards, and D. Fäh. Reference s-wave velocity profile and attenuation models for ground-motion prediction equations: application to japan. *Bull. Seism. Soc. Am.*, 103:2645–2656, 2013b.

S. Rezaeian, Y. Bozorgnia, I.M. Idriss, N.A. Abrahamson, K.W. Campbell, and W.J. Silva. Damping scaling factors for vertical elastic response spectra for shallow crustal earthquakes in active tectonic regions: "average" horizontal component. *Earthquake Spectra*, 30:939–963, 2014.

S. Wiemer, J. Hiemer, S. adn Woessner, L. Danciu, D. Fäh, B. Edwards, C. Cauzzi, C. Michel, V. Poggi, E. Kissling, P. Kaestli, and D. Giardini. The 2014 update of the swiss national seismic hazard model - key science issues. *2ECEES Istanbul*, 2014.